also isolated cDNA clones for human and mouse homologs and identified spliced variants of mRNA for each species. Kdap mRNA was expressed specifically in the suprabasal layer of embryonal and neonatal rat skin. Because of Kdap's specific expression in skin and the possibility that it is secreted, we hypothesized Kdap to contribute to the regulation of human epidermal structure and/or function. Thus, we examined Kdap expression in human skin and other tissues, and characterized its biochemical properties and the regulation of gene expression during keratinocyte differentiation and of *in situ* protein expression in normal and psoriatic skin. Our findings expand our knowledge of Kdap, serving as the basis for further investigation into its function within epithelial tissue.

Results

Molecular cloning of novel SS-encoding genes expressed selectively by keratinocytes To identify novel genes encoding secreted proteins expressed selectively by keratinocytes, we employed an SS trap (Tashiro *et al*, 1993) and differential colony hybridization. Because SS is encoded by 5′-end cDNA sequences, these sequences were enriched from cDNA synthesized with mRNA from primary-cultured human keratinocytes. We then inserted enriched cDNA into an expression vector to produce a fusion protein of cDNA-encoded polypeptide and SS-deficient hIL-2Rα. This cDNA library was transferred into COS-1 cells and examined for the ability of cDNA to escort hIL-2Rα-lacking SS to the cell surface, as judged by surface staining using anti-hIL-2Rα antibody (Ab) (Bonkobara *et al*, 2003). cDNA clones exhibiting surface expression were screened further using differential colony hybridization (Ariizumi *et al*, 1997) for genes expressed by keratinocytes, but not by dermal fibroblasts. These procedures yielded six novel genes (found in the EST database updated in the year of 2000) encoding SS that hybridized strongly with total cDNA probes prepared from keratinocyte mRNA, but only marginally or not at all with dermal fibroblast probes. Finally, full-length cDNA clones for each of the six EST genes were isolated and their entire nucleotide sequences were determined (Bonkobara *et al*, 2003).

Amino acid structure of an EST clone Among the six EST genes was one encoding a polypeptide (termed Kdap) consisting of 99 amino acids with a putative N-terminal SS of 22 amino acids (Fig 1). Comparison with known proteins in the human GenBank database (updated in 2000) failed to identify homologous proteins, but an EST database search revealed mouse and rat homologs (note that these sequences were not full-length cDNA clones). Indeed, we were able to clone the cDNA for these homologs using RT-PCR of mRNA from mouse and rat skin, respectively; nucleotide sequences were confirmed by comparison with EST clones. Analysis of amino acid sequences showed considerable conservation among the three species (54%–59% identity) (Fig 1). By contrast, the *IYP* sequence (located just after the SS) was found only in the mouse. A homology search conducted in 2003 revealed that our isolated gene is identical to Kdap, previously reported by Oomizu *et al* (2000).

Keratinocyte-predominant expression of Kdap mRNA As expected, northern blotting of the Kdap gene showed a transcript of approximately 1 kb expressed by keratinocytes, but not by dermal fibroblasts (Fig 2*A*). Human mRNA was detected only in the skin at a high level and in the thymus at a considerably lower level. Similar tissue specificity was noted for mouse mRNA (Fig 2*B*). We next examined RNA expression in different epithelia using RT-PCR (Fig 2*C*); there was high expression in oral mucosa, tongue, esophagus, and stomach, similar to that in the skin; much lower expression in the bladder and uterus; and no expression in the gastrointestinal mucosa. These results indicate that Kdap mRNA is expressed by various epithelia, especially those predominantly populated by keratinocytes.

Kdap is a secreted protein To determine whether the N-terminal amino acid sequence of Kdap acts as an SS to permit its secretion, we transfected an expression vector (pKdap-Fc) encoding a fusion protein of the entire Kdap sequence and the Fc portion of human IgG1 into COS-1 cells, and then harvested the supernatant (extracellular fraction) and whole-cell extracts (intracellular fraction) separately. Protein expression was determined by western blotting using anti-human IgG Ab (Fig 3*A*). Whereas Kdap-Fc protein was detected clearly as a single band of 49 kDa in the extracellular fraction, it was barely detectable in the intracellular fraction (control Ab did not produce specific bands), indicating that protein is secreted efficiently and also suggesting that the N-terminal sequence acts as an SS in transfected cells. To map the SS cleavage site, we used protein A-affinity chromatography to purify the Fc-fusion protein from the supernatant and automated Edman degradation to determine N-terminal amino acid residues. Our results indicated that the secreted Fc-fusion protein starts at alanine on amino acid 23, the cleavage site lying between this amino acid and glycine on amino acid 22 (Fig 1).

For biochemical characterization, we immunized rabbits with His-tagged recombinant Kdap protein (His-Kdap) to produce anti-human Kdap Ab. This Ab was used to examine Kdap secretion (without tags) in COS-1 cells that were gene transferred using an Adv with full-length Kdap cDNA (Fig 3*B*). By western blotting, we detected a single band of 12.5

```
                                    ▽
Kdap_H MKIPVLPAVVLLSLLVLHSAQGATLGGPE--EESTIENYASRPEAFNTPF 48
Kdap_M MKIPILPVVALLSLLALHAVQGAALGHPTIYPEDSSYNNYPTATEGLNNEF 51
Kdap_R MKIPILPIVALLSLLALHAAQGAALGTPM---EDTTSSNYPSGTEGLS-EF 47

Kdap_H LNIDKLRSAFKADEFLNWHALFESIKRKLPFLNWDAFPKLKGLRSATPDAQ 99
Kdap_M LNFKRLQSAFQSENFLNWHVITDMFKNAFPFINWDFFPKVKGLRSAAPDSQ 102
Kdap_R LNFNKLQSAFKSDDFLNWHVLTDMFKKALPFINWEFFPKVKGLRSAVPDSQ 98
```

Figure 1
Amino acid sequences of human keratinocyte differentiation-associated protein (Kdap). Amino acid sequence (deduced from nucleotide sequences of human Kdap cDNA, Kdap_H, GenBank accession number *XM_097406*) is aligned with those of mouse (Kdap_M, W30505) and rat (Kdap_R, AB011028) homologs. Human Kdap precursor is cleaved between amino acid 22 and 23 (shown by a reverse triangle).

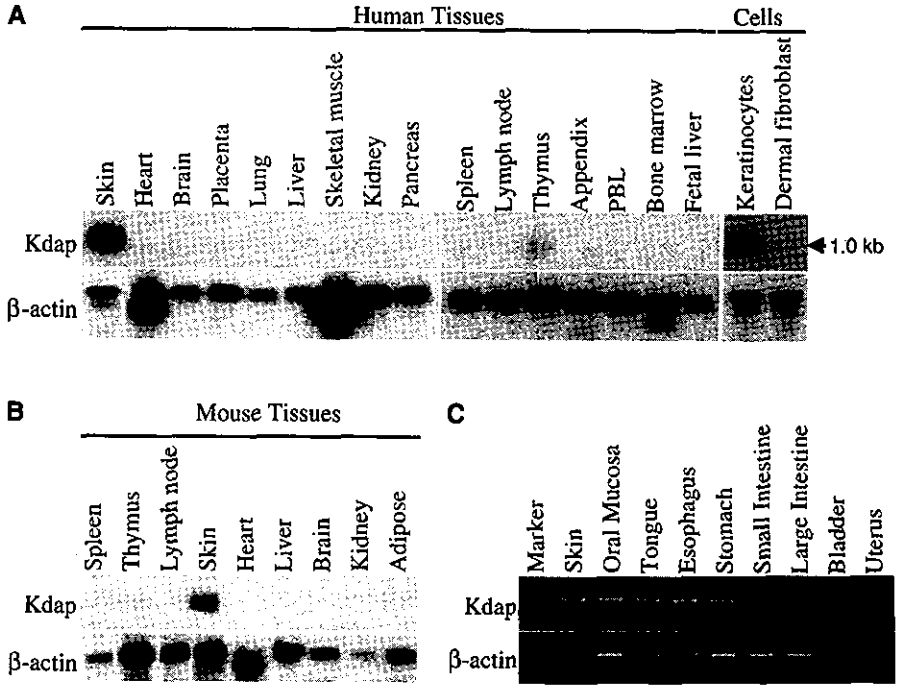

Figure 2
mRNA expression of human and mouse keratinocyte differentiation-associated protein (Kdap). mRNA isolated from primary-cultured cells and various human (*A*) and mouse (*B*) tissues was examined by northern blotting for mRNA expression of Kdap or β-actin. Expression was also assayed using RT-PCR of RNA isolated from different mouse epithelial tissues using RT-PCR (*C*).

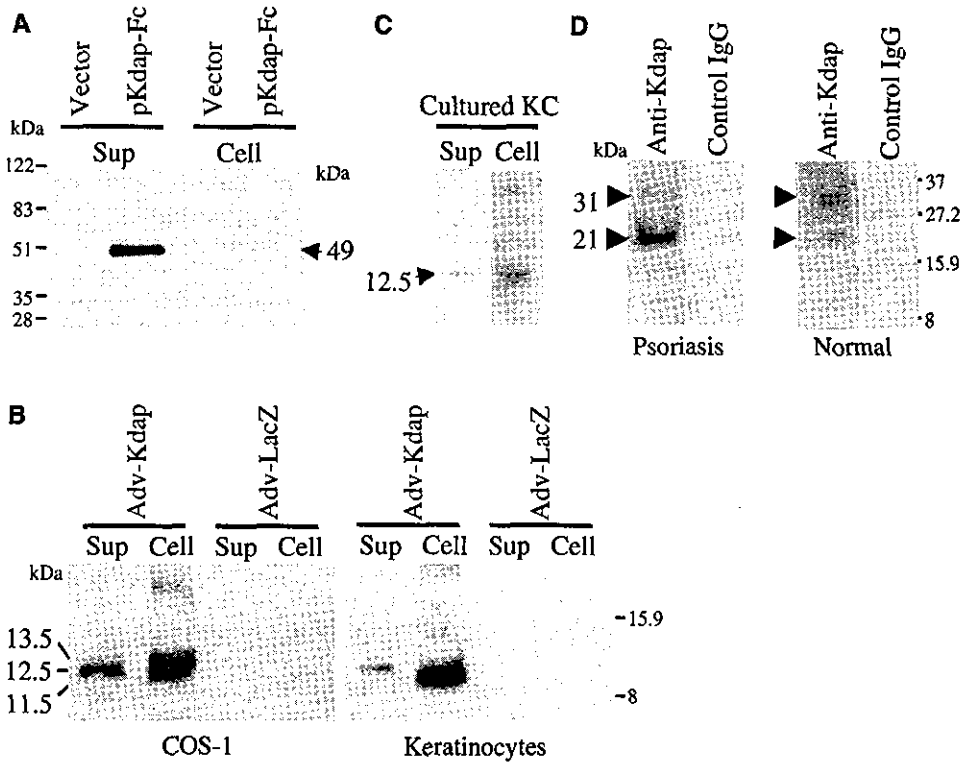

Figure 3
Protein expression of human keratinocyte differentiation-associated protein (Kdap). Human Kdap protein was characterized by western blotting of culture supernatant and protein extracts prepared from Kdap gene-transfected cells, primary-cultured keratinocytes, psoriatic or normal scales. (*A*) COS-1 cells were transfected with an empty vector (Vector) or an expression vector (pKdap-Fc) encoding for a fusion protein of the entire sequence of human Kdap (including a signal sequence) and Fc portion of immunoglobulin. At 2 d post-transfection, the culture supernatant (Sup) was harvested and whole-cell extracts (Cell) were prepared. Aliquots (10% each fraction) were subjected to SDS-PAGE analysis followed by western blotting, using anti-human IgG Ab. (*B*) COS-1 cells (*left panel*) or keratinocytes (*right panel*) were infected with recombinant Adv encoding Kdap (Adv-Kdap) or LacZ gene (Adv-LacZ). Likewise, the small aliquots (5% and 10% for COS-1 cells and keratinocytes, respectively) were examined for expression of Kdap protein. (*C*) Whole-cell extracts were prepared from primary-cultured keratinocytes and the supernatant was harvested and concentrated 10–20-fold. Small aliquots (10% each) were applied for SDS-PAGE. (*D*) Crude extracts (75 μg) prepared from scales psoriatic or normal scales were assayed by western blotting, using anti-human Kdap Ab or control rabbit IgG.

kDa in the extracellular fraction and two bands (13.5 and 11.5 kDa) in the intracellular fraction (no bands were detected with control Ab). The latter bands most likely correspond to a precursor containing SS and the mature form, respectively. Ab specificity was confirmed by the absence of detectable bands in the two fractions of COS-1 cells infected with Adv-LacZ (expression vector for β-galactosidase gene). We noted the extracellular mature form (12.5 kDa) to be slightly larger than the intracellular mature form (11.5 kDa); both mature forms were markedly larger than the size predicted from the primary amino acid sequence (8.7 kDa). Similar differences in molecular weights were also detected using Adv-infected keratinocytes (Fig 3*B*). Kdap protein was found mostly in the intracellular fraction, although lower levels were detected in the supernatant, indicating that secretion was blocked partially in these infected keratinocytes. This low secretion may be due to lack of mature lamellar granules (secretory vesicles) in *in vitro* cultured keratinocytes (undifferentiated phenotype). In primary-cultured keratinocytes in which Kdap is synthesized from the endogenous gene (rather than from the transgene), only small amounts of protein were detected in both extracellular and intracellular fractions when more proteins and longer exposure to an X-ray film were involved (Fig 3*C*). Nonetheless, secretion of Kdap was proved by cleavage of N-terminal sequence and detection of Kdap protein in culture supernatants of transfected (transgene expression) and non-transfected keratinocytes (endogenous gene expression).

We also examined protein expression of Kdap in crude extracts prepared from scales of psoriatic or normal skin (not cultured cells) (Fig 3*D*). Western blotting using the same Ab detected two bands in the extracts of psoriatic scales: a thicker band (21 kDa) and a thinner band (31 kDa). These molecular weights were about two to three times larger than the 11.5 kDa detected in the cell extracts of non-transfected and transfected keratinocytes (Fig 3*B*). In normal scales, both bands were also detected, but expression levels were much lower than in psoriatic scales, suggesting upregulated expression of Kdap *in situ* in psoriatic skin. Moreover, the ratio of the two bands' intensities was converse to that found in psoriatic scales. Variations in the molecular weight of the secreted (matured) Kdap protein were not detected. By contrast, intracellular Kdap appears to vary, most likely due to post-translational modification.

***In situ* expression in human skin** Using the previous Ab, we examined Kdap expression in normal human skin. Indirect immunofluorescence highlighted the upper spinous and granular layers on control cryostat sections of the human epidermis (see arrows in Fig 4*A*). Staining was predominantly observed in an alternate wave-like pattern, with the strongest staining at the apical edges of the granular cells (inset in Fig 4*A*). There was little or no staining of the cornified layer and very weak staining was occasionally seen in the mid-epidermal layers. By contrast, in lesional skin of psoriatic patients, Kdap was expressed more widely and at high levels throughout suprabasal keratinocytes (Fig 4*B*). This expression pattern in psoriasis is similar to that reported for SKALP/elafin (Pfundt *et al*, 1996) and for cystatin M/E (Zeeuwen *et al*, 2001), both of which are low-molecular-weight and secreted proteins with anti-proteinase activity. It should be noted that this more widespread Kdap expression in psoriasis was not seen in other cornification disorders, such as the bullous and non-bullous types of congenital ichthyosiform erythroderma, lamellar ichthyosis with or without TGM1 mutation, and palmoplantar keratoderma.

We next examined Kdap mRNA expression in normal skin using *in situ* hybridization (Fig 4*C*). Unlike its protein expression, Kdap mRNA was detected more widely throughout suprabasal keratinocytes. This difference between protein and mRNA expression is reminiscent of involucrin, an established marker of keratinocyte differentiation (de Viragh *et al*, 1994). Consistent with the protein expression, Kdap was not expressed by basal keratinocytes, strongly suggesting that Kdap is also a marker of keratinocyte differentiation.

Kdap is secreted into the extracellular space via lamellar granules To determine the ultrastructural localization of Kdap in granular keratinocytes, we conducted immunoelectron microscopic analysis of normal human epidermis stained with anti-Kdap Ab and gold particle-conjugated anti-rabbit IgG (Fig 5). Kdap staining localized to areas immediately beneath the apical side of the keratinocyte

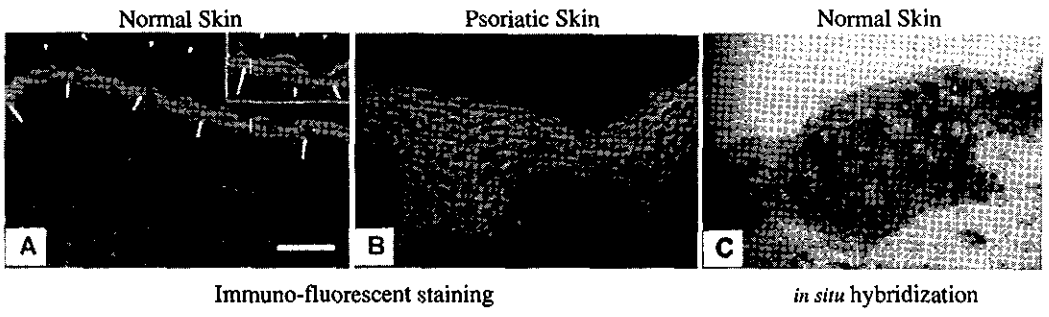

Figure 4
Keratinocyte differentiation-associated protein (Kdap) expression in normal and psoriatic skin. Frozen skin sections prepared from normal healthy adults (*A*, *C*) and psoriatic patients (*B*) were immunofluorescently stained with anti-Kdap Ab and fluorescein isothiocyanate-conjugated anti-rabbit Ab (*A*, *B*) or hybridized *in situ* with anti-sense RNA probe for the Kdap gene (*C*). A higher magnification is provided in inset (*A*). The granular layer and stratum corneum are indicated by arrows and arrowheads, respectively (*scale bar*: 50 mm). No staining was observed with control rabbit IgG or sense RNA probe. Data shown are representative of staining of skin biopsies from three individuals with psoriasis.

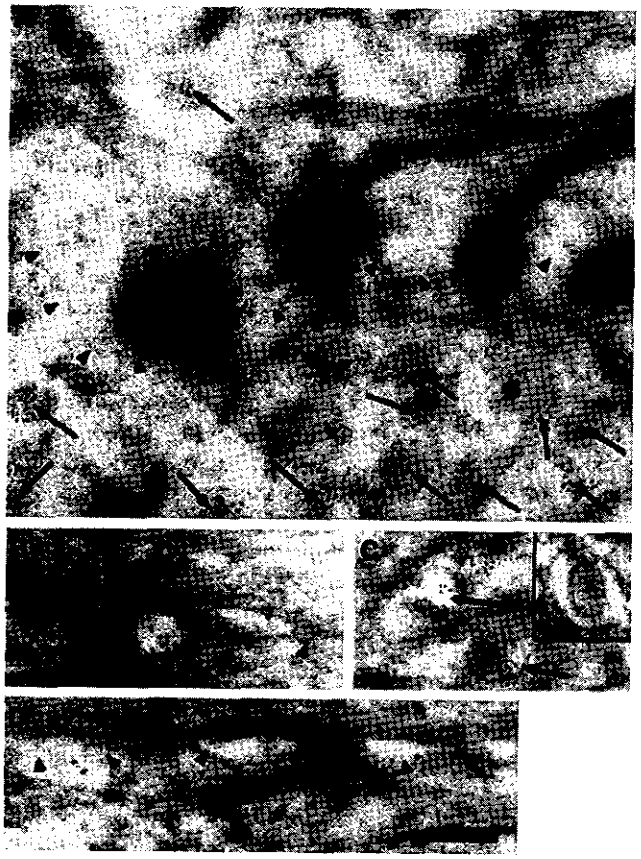

Figure 5
Keratinocyte differentiation-associated protein (Kdap) protein is localized to lamellar granules of keratinocytes. After staining normal skin with anti-Kdap Ab and secondary Ab conjugated with gold particles, localization of Kdap protein ultrastructually was examined in the granular keratinocytes. (*A*) Low magnification: immuno-gold label (representing Kdap) was found in small vesicles under the apical plasma membrane of granular keratinocytes (*arrows*), a localization similar to that of lamellar granules. Some labeled granules were also seen fusing with or in close association to the plasma membrane. (*B*) Kdap was also present in the intercellular space. (*C*) Higher magnification: although membrane-bound vesicles failed to show the classic lamellar characteristics of membrane coating granules seen in routine transmission EM sections, the size and frame structure were identical to those of lamellar granules (inset). Multiple clusters of lamellar granule-like vesicles were localized within elongated, electron-lucent areas of the cytoplasm just under the plasma membrane (*arrows*). (*D*) Kdap was observed close to or on the cell membrane (*arrowheads*) of granular keratinocytes (*scale bars*: 2a 50 nm, 2b, c and d 100 nm).

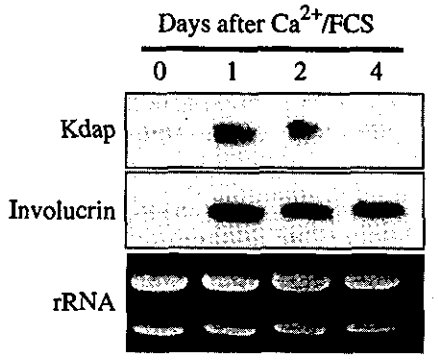

Figure 6
Expression of keratinocyte differentiation-associated protein (Kdap) mRNA is markedly induced during *in vitro* keratinocyte differentiation. At indicated time points after inducing differentiation with high-dose Ca^{2+}, total RNA was isolated from treated cells and examined by northern blotting for Kdap and involucrin mRNA expression. Amounts of ribosomal RNA (rRNA) detected by ethidium bromide staining were similar in all four RNA samples.

plasma membrane in the upper suprabasal and granular layers (Fig 5). These areas were rich in apparently membrane bound vesicles containing both variably electron dense material that was consistent with them being membrane-coating granules (lamellar granules). These granules could sometimes be seen closely arranged together in a distinctive pattern beneath the plasma membrane. By contrast, there were very few Kdap-labeled vesicles in the region directly above the plasma membrane (Fig 5*A*). The position of the labeling was over both the vesicle plasma membrane and the center of the vesicle (Fig 5*A–C*). The morphology of the cryofixed and substituted control skin often, but not always, failed to reveal the fine detail of the membrane coating (lamellar) granules as seen by conventional EM (Fig 5*C*). Both the size of the vesicles stained by anti-Kdap Ab and their distribution pattern within granular keratinocytes strongly suggests that Kdap is in the lamellar granules or their contents. The Kdap-containing granules were seen close to the plasma membrane, and Kdap staining was also observed in the intercellular space (Fig 5*B* and *D*). Morphometric analysis of Kdap labeling (>750 gold particles) at the outer surface of the plasma membrane in the upper granular keratinocyte layers showed a significant proportion (40%) of labeling on or between the external surfaces of the plasma membrane or between granular cells in the intercellular spaces (the majority of the remaining 60% of plasma membrane labeling was restricted to the lamellar granules subjacent to the apical plasma membrane (Fig 5*B* and *D*). These results indicate that Kdap is secreted by differentiated keratinocytes and may be incorporated into the lipid layer and the external surface of the CCE.

Kdap mRNA expression is upregulated markedly during keratinocyte differentiation *in vitro* To examine the effect of keratinocyte differentiation on Kdap mRNA expression, we cultured keratinocytes in low-Ca^{2+} media to maintain these cells in a basal state, and then induced differentiation by shifting to high-Ca^{2+} media containing 10% FCS. Time-dependent changes in mRNA expression were assessed by northern blotting, and keratinocyte differentiation was monitored in parallel by involucrin mRNA expression. In low-Ca^{2+} media, both Kdap and involucrin were expressed at background levels (Fig 6). After shifting to high-Ca^{2+} media, involucrin mRNA was increased markedly after 24 h and this high level was maintained for 4 d. Kdap mRNA was also upregulated at 24 h (60-fold higher than in untreated keratinocytes), but unlike involucrin, Kdap's upregulated expression lasted for only 2 d. These results indicate that Kdap (like involucrin) is a marker of keratinocyte differentiation; however, Kdap and invlucrin differ in the kinetics of mRNA expression during differentiation *in vitro*.

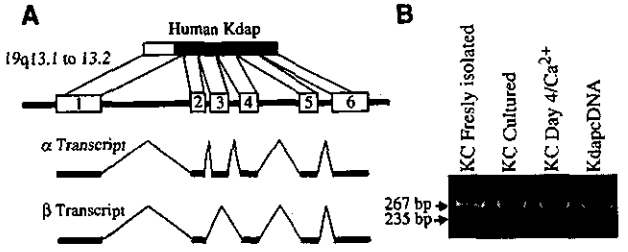

Figure 7
Human β transcript is generated by alternative splicing mechanisms. (*A*) The organization of human keratinocyte differentiation-associated protein (Kdap) gene on chromosome 19q13.1 to 13.2 is represented schematically. The nucleotide sequence of α transcript (a full-length form) segmented into six exons, and aligned to that of β transcript with deletion of exon 3. (*B*) Total RNA was isolated from keratinocytes that were freshly isolated from neonatal foreskin tissue, primary cultured, or treated with high Ca^{2+} medium (day 4). RNA was examined for mRNA expression of α and β transcripts by RT-PCR using a primer set (Materials and Methods). Full-length Kdap cDNA was also PCR amplified as control. PCR products were then size-fractionated through 8% native PAGE and stained with ethidium bromide.

A spliced variant is produced by alternative splicing mechanisms In isolating a full-length cDNA clone for Kdap (α transcript), we identified an additional cDNA clone containing a shorter insert (termed β transcript) (Fig 7*A*). Nucleotide sequence analysis showed that the coding sequence of the β transcript is identical to an alternatively spliced form (GenBank accession number AA58342) that was reported by Oomizu *et al*. Note, however, that the two transcripts differ in their 3′-untranslated region. Amino acid sequence deduced from the DNA sequences revealed a deletion of amino acid 43–56. We also examined expression levels of β transcript relative to a transcript in keratinocytes by RT-PCR using a primer set designed to amplify a 267 bp fragment for a transcript and a 235 bp for β transcript (Fig 7*B*). In addition to a 267 bp fragment, a band corresponding to a 235 bp was noted. This band was very faint in PCR products of RNA from keratinocytes freshly isolated from skin, and was unchanged in primary-cultured keratinocytes induced to differentiate after treatment with high-Ca^{2+} media. These results show that the spliced variant of Kdap mRNA is not the major transcript in keratinocytes.

To determine whether this spliced variant was generated by alternative splicing mechanisms, we searched for the Kdap gene in the human genome database (provided by NCBI). An entire sequence of Kdap cDNA segmented into six exons was found in the locus between 13.1 and 13.2 on chromosome 19 (Fig 7*A*): exon 1 encoded for the SS and a part of N-terminal mature Kdap; and other five exons encoded for the rest of the amino acid residues. The 5′- and 3′-flanking sequences of each exon contained conserved splice acceptor/donor sequences. A nucleotide sequence missing from the β transcript was identical to exon 3, indicating that the β transcript was generated by alternative splicing (exon skipping).

Discussion

Kdap was first identified by Oomizu *et al* (2000) by suppression subtractive cDNA cloning of skin from rats at different embryonal stages of hair differentiation (prehair-germ *vs* hair-germ stages). They also identified mouse and human homologs and their spliced variants. Expression studies in rat showed that: (1) Kdap mRNA was induced after the hair-germ stage (quantitative RT-PCR); (2) its expression was restricted to epithelial tissues in rat embryo tissues (RT-PCR); and (3) skin expression was confined to the suprabasal layers of embryonal epidermis (*in situ* hybridization).

At the time we initiated our studies, Kdap was not registered in the GenBank database nor were Oomizu's results published. Employing a different strategy, we coupled an SS trap with differential colony hybridization and isolated the same gene from a cDNA library constructed with mRNA from primary-cultured human keratinocytes. Using a wide spectrum of human and mouse tissues and northern blotting, we affirmed the epithelium-specific expression of Kdap and its suprabasal layer-specific expression within the epidermis. We did note the new finding of low-level expression by human thymus (Figs 2 and 4*C*).

Expanding on the findings of Oomizu *et al* we found that: (1) human Kdap is secreted by keratinocytes (N-terminal amino acid sequence functioned as an SS; Kdap protein was detected in the extracellular fraction of transfected and non-transfected keratinocytes (Fig 3); and it resided in lamellar granules of granular keratinocytes and the intercellular space of the stratum corneum (Fig 5); (2) Kdap protein is confined to the granular layer of normal epidermis (which is not identical to its mRNA expression pattern); (3) expression in psoriatic skin is more diffuse, involving suprabasal layers; (4) mRNA expression is regulated by keratinocyte differentiation; and (5) spliced variant is produced by alternative splicing mechanisms and expressed in keratinocytes only at very low levels (in contrast to the full-length form).

We observed variation in the molecular weight of Kdap protein. The molecular weight of Kdap produced by transfected cells was larger than that predicted from the primary amino acid sequence (Fig 3*B*). This is due most likely to post-translational modification in which fatty acids, glycosylphosphatidylinositol (GPI) (Chatterjee and Mayor, 2001), or other small sized molecules are incorporated. Glycosylation may not take place because Kdap contains neither possible *N*-glycosylation sites nor putative *O*-glycosylation sites (e.g., proline-, serine-, threonine-rich regions) (Wilson *et al*, 1991). We also observed another type of modification. The molecular weight of Kdap in crude extracts from psoriatic and normal skin was two to three times larger than that detected in transfected and non-transfected keratinocytes (Fig 3C). This finding suggests that Kdap is polymerized or cross-linked to polymerized proteins in the skin. Because polymerization was not found in the extracellular Kdap proteins, we speculate that Kdap is anchored to structural proteins by TGase inside keratinocytes, as has been shown for elafin and cystatins (Zeeuwen *et al*, 2001; Nakane *et al*, 2002). But we could not document TGase-dependent cross-linking of Kdap (data not shown), which may mean that Kdap polymerization is achieved by other mechanisms.

Since highly polymerized Kdap cannot be solubilized using our buffer containing Triton X-100 detergent, we may have lost the majority of Kdap protein during protein

extraction. This possibility may thus account for poor expression of Kdap (in western blotting) in intracellular fractions of non-transfected primary-cultured keratinocytes (Fig 3*C*) and also explain the poor efficiency of secretion by keratinocytes.

Recent molecular studies on CCE components have documented the presence of low-molecular-weight secreted proteins in the protein envelope consisting of an insoluble complex of proteins, which include SKALP/elafin (Schalkwijk *et al*, 1990; Wiedow *et al*, 1990), secretory leukocyte proteinase inhibitor (SLPI) (Jin *et al*, 1997), lympho-epithelial Kazal-type-related inhibitor (LEKTI) (Mägert *et al*, 2001) cystatin A and M/E (Takahashi et *al*, 1992; Sotiropoulou *et al*, 1997a, b; Zeeuwen *et al*, 2001), plasminogen activator inhibitor-type 2 (PAI-2) (Lavker *et al*, 1998), and bikunin (Cui *et al*, 1999). All these proteins possess activity to inhibit either serine or cysteine proteinases, some of which are further characterized by restricted expression to keratinocytes. These inhibitors have been proposed to play a pivotal role in regulating renewal of the epidermis and protecting the epidermis from tissue damages by suppressing activities of endogenous and exogenous proteinases.

Kdap shares some attributes with these epidermal proteinase inhibitors, including being a low-molecular-weight secreted protein and showing a restricted expression to granular keratinocytes (or CCE). By contrast, Kdap appears unique with respect to its localization within lamellar granules and the existence of naturally occurring spliced variants producing truncated isoforms. In addition, Kdap might be efficiently secreted by granular keratinocytes (Fig 5), suggesting that it may function as a soluble regulator in the extracellular space.

Because of the similarities to epidermal proteinase inhibitors, we hypothesized that Kdap possesses activity to inhibit proteinase and/or growth of microbes. Purified His-Kdap and His-DHFR were used to determine whether Kdap could inhibit the activity of cysteine proteinases (papain, ficin, and cathepsin B) and serine proteinases (chymotrypsin and trypsin). His-Kdap (10 μM) inhibited the proteinase activity of papain (100 nM) almost completely, whereas His-DHFR at the same concentration failed to do so (data not shown). Although we found anti-proteinase activity of Kdap, the activity appears 10–100-fold lower than those for other epidermal inhibitors (e.g., cystatin M/E; Sotiropoulou *et al*, 1997). Secondly, His-Kdap was assayed for activity to suppress the growth of microbes (*Streptococcus group A*, *E. coli*, *Staphylococcus aureus*, and *Candida albicans*). No suppressive activity was found with any of the microbes tested. Kdap is thus likely to possess disparate function from other low-molecular-weight secreted proteins in the CCE, although there remains the possibility that post-translational modification is required to activate Kdap function (His-Kdap produced in *E. coli* assumed to have no modification similar to that in keratinocytes).

Materials and Methods

Cell culture Primary keratinocytes and dermal fibroblasts were isolated, respectively, from epidermis and dermis of newborn human foreskins as described before (Girolomoni *et al*, 2000). Isolated keratinocytes were maintained and expanded in keratinocyte-SFM media (Invitrogen, Carlsbad, California). Third- to sixth-passaged keratinocytes (60%–80% confluency) served as a source of RNA for cDNA library construction and for experiments examining gene expression. Dermal fibroblasts and COS-1 cells were cultured in Dulbecco's modified Eagle's medium (DMEM) supplemented with 10% fetal calf serum (FCS).

Cloning of keratinocyte-specific and SS-encoding genes For the SS trap, we constructed a cDNA library based on a report by Tashiro *et al* (1997). We fused 5′-end cDNA sequences from keratinocyte mRNA in frame to the gene for a variant human interleukin-2 receptor α (hIL-2Rα) lacking SS in order to produce hIL-2Rα fusion proteins. Eight thousand independent colonies were sorted randomly from the library into 163 pools (49 clones per pool) for SS trap screening (Tashiro *et al*, 1997; Bonkobara *et al*, 2003). Plasmid DNA (0.2 μg) from each pool (all colonies in a group) was transfected into COS-1 cells (1×10^4) seeded on eight-well chamber slides (NUNC, Naperville, Illinois) using FuGENE 6 (Roche Molecular Biochemicals, Indianapolis, Indiana). After 3 d of culture, the transfectants were assayed by immunocytochemistry for surface expression of hIL-2Rα; fixed cells were incubated with 0.5 μg per mL of mouse monoclonal antibody (mAb) against hIL-2Rα (R&D Systems Inc., Minneapolis, Minnesota). After incubation with biotinylated anti-mouse IgG, avidin-peroxidase and 3-amino-9-ethylcarbazole (AEC) (DAKO, Carpinteria, California) were applied and the color stain was examined under light microscopy. Pools showing surface expression of IL-2Rα were sub-divided (7 clones per subpool), and then screened further in the above manner. Finally, cDNA clones in positive subpools were examined clonally for IL-2Rα surface expression.

cDNA clones with IL-2Rα surface expression were screened by differential hybridization as described previously (Arilzumi *et al*, 1997, 2000) for cDNA expressed selectively by keratinocytes. Selected colonies (193 clones) were transferred to nylon membranes and hybridized with total cDNA probes prepared from poly(A)$^+$ RNA of keratinocytes or with total cDNA probes of dermal fibroblasts. This differential hybridization led to selection of 36 cDNA clones with strong hybridization signals for keratinocyte total cDNA probes, but little or no signals for dermal fibroblast probes.

The SS-trapped cDNA clones expressed selectively by keratinocytes were examined for nucleotide sequence identities in GenBank and EST databases using a Blast search program from the National Center for Biotechnology Information (NCBI). cDNA clones found in the EST database were evaluated for full-length nucleotide sequences (SS-trapped cDNA clones contain 5′-end sequences only) using 3′ rapid amplification of cDNA ends (3′ RACE) system (Invitrogen). The clones with longest cDNA inserts were selected and their nucleotide sequences were determined.

Northern blotting and RT-PCR analysis Northern blotting was performed as described previously (Arilzumi *et al*, 1995). Poly(A)$^+$ RNA (2 μg) isolated from primary-cultured human keratinocytes, dermal fibroblasts, foreskins, and mouse organs were size-fractionated on a vertical agarose gel, transferred electrophoretically onto a nylon membrane, and hybridized in buffer containing 1×10^6 c.p.m. per mL of ^{32}P-labeled cDNA for Kdap or β-actin gene. After incubating for 16 h at 42°C, membranes were washed and autoradiographed. For tissue distribution of human Kdap mRNA, a nylon membrane (Human Multiple Tissue Blots purchased from BD Biosciences, Palo Alto, California) with an array of mRNA (2 μg) isolated from various human organs was hybridized according to the manufacturer's recommendations.

To determine Kdap gene expression in total RNA isolated from mouse epithelial tissues, RT-PCR was performed (Arilzumi *et al*, 1995). RNA (100 ng) was reverse-transcribed and then PCR-amplified in one tube (50 μL) containing 0.2 mM dNTP, 1.2 mM

$MgCl_2$, 20 pmol primers, and SuperScript II RT/Taq mix (Superscript One-Step RT-PCR System, Invitrogen) using a protocol for cDNA synthesis (45°C for 30 min, and then at 94°C for 2 min). The PCR cycling protocol included incubation at: 94°C for denaturation (45 s); 60°C for mouse Kdap or 55°C for β-actin primers for annealing (45 s); 72°C for extension (60 s); and 30 cycles. PCR products (20 μL) were size-fractionated electrophoretically on 1.2% agarose gel and visualized by ethidium bromide staining. The following primers were used to PCR-amplify cDNA: for mouse Kdap, 5′-CAGCCCAAACCGGACACCAT-3′ and 5′-GGGGAACTGAGGCAAGGAAGATTT-3′; and for mouse β-actin, 5′-GAGCGGGAAATCGTGC GTGACATT-3′ and 5′-GAAGGTAGTTTCGTGGATGCC-3′.

For experiments examining the expression of alternatively spliced Kdap mRNA in keratinocytes, we used the same conditions as before, except for a different annealing temperature (58°C) and a primer set: 5′-CTGCCGTGGTGCTCCTCTCC-3′ and 5′-AGTTGCGCTCCTCAGTCCTTTCA-3′.

Construction of plasmid and adenoviral expression vectors A plasmid expression vector, pKdap-Fc, encoding a fusion protein of human Kdap precursor and an Fc portion of human IgG1, was constructed. Briefly, the entire coding sequence for Kdap precursor was PCR amplified with 5′- and 3′-primers containing *EcoRI* and *XbaI* restriction enzyme sites, respectively. The resulting PCR fragment was inserted in frame into the 5′-end of a coding sequence for the Fc portion that had been subcloned previously into a CMV-driven expression vector (pcDNA3.1, Invitrogen).

Adenoviral vectors (Adv) were generated according to the manufacturer's manuals of AdEasy system (Quantum Biotechnologies, Carlsbad, California) with minor modifications (He *et al*, 1998). A full-length cDNA for the human Kdap precursor was introduced into a CMV-driven shuttle vector (pShuttle-CMV) using *XhoI* and *EcoRV* restriction sites. After linearization of the shuttle vector DNA with *PmeI*, DNA (0.5 μg) was co-transformed into BJ5183 *Escherichia coli* (Quantum Biotechnologies) with 0.1 μg of pAdEasy-1, which encodes a whole genome of Adv type 5 lacking the E1 and E3 regions. The obtained plasmid clones were screened for recombinant Adv DNA by total size (>33 kb) and by presence of the Kdap gene. A plasmid sequence in a selected recombinant DNA (5 μg) was removed by digestion with *PacI* and then transfected into a permissive cell line, 293A, using 6 μg of FuGENE 6. After culturing for 6 d, recombinant viral particles were recovered by freeze–thawing transfected cells, amplified further by infection of large numbers of 293A cells, and then purified by double ultracentrifugation through cesium chloride gradients. Plaque-forming units (PFU) of purified Adv were determined using the tissue culture infectious dose ($TCID_{50}$) method described previously (He *et al*, 1998).

Gene delivery In plasmid transfection, COS-1 cells were seeded at 1 d prior to transfection onto a 60 mm culture dish at a density of 5×10^5 cells. Cells were incubated overnight in the presence of the expression vector DNA (2 μg) and 6 μL of FuGENE 6. For Adv-mediated gene delivery to COS-1 cells and keratinocytes, cells were seeded on 24-well plates at a density of 1×10^5 cells per well. The next day, recombinant Adv was added at multiplication of infection (MOI) of 250 for COS-1 cells and 500 for keratinocytes. After incubating at 37°C for 90 min, uninfected Adv was washed out and then cultured for 2 d.

Extraction of proteins and SDS-PAGE/western blotting Two days after transfection or infection, the culture medium was replaced with fresh medium. The next day, the supernatant was recovered and whole-cell extracts were prepared by incubating cells with 0.3% Triton X-100/phosphate-buffered saline (PBS) containing 1 mM phenylmethylsulfonyl fluoride (PMSF) and 2 μg per mL of leupeptin, followed by centrifugation (Shikano *et al*, 2001). Whole-cell extracts were also prepared from the scales of psoriatic skin and of dry skin in a healthy individual as described previously (Zeeuwen *et al*, 1997). In experiments assaying Kdap protein expression from the supernatant of cultured keratinocytes (not transfected), the supernatant was concentrated in volume 10–20-fold by lyophilization and subsequently rehydrated with a small volume of buffer.

Aliquots of each fraction prepared from transfected cells or protein extracts from psoriatic scales were size fractionated on 16.5% Tris-Tricine gels under reduced conditions. Following electro-transfer onto Hybond-P membrane (Amersham Pharmacia Biotech, Piscataway, New Jersey), the membranes were blocked with 5% non-fat dried milk/0.1% Tween 20/PBS and incubated with 0.1 μg per mL of purified rabbit IgG raised against His-tagged Kdap recombinant proteins or control IgG. Signals were developed with horseradish peroxidase (HRP)-conjugated goat anti-rabbit IgG and ECL plus system (Amersham Pharmacia Biotech).

Production of antibodies against His-tagged recombinant Kdap protein A bacterial expression vector, pET-hKdap, was constructed by insertion of a PCR-amplified coding sequence for human mature Kdap in frame into that for N-terminal 10 × Histidine in an expression vector, pET-16b (Novagen, Madison, Wisconsin). BL21(DE3) *E. coli* (Novagen) transformed with pET-hKdap was treated with 1 mM IPTG for 6 h. After harvesting cells, whole proteins were extracted by 8 M urea/100 mM sodium acetate/Tris-HCl, pH 8.0, and applied to affinity purification with nickel resins (Quiagen). His-tagged Kdap was eluted from the resins with 8 M urea/100 mM sodium acetate/0.5 M imidazole, pH 4.5, fractions were collected containing proteins, and finally refolded by dialysis against 100 mM phosphate buffer (pH 7.7).

Refolded His-Kdap was used for immunization of rabbits. A mixture of Kdap recombinant proteins (200 μg per rabbit) and complete Freund's adjuvant was injected into rabbits, followed by three boosts with incomplete Freund's adjuvant at 3-wk intervals. Five days after the last boost, serum was collected from immunized rabbits and affinity purified with beads conjugated with His-Kdap.

N-terminal sequencing To determine the exact site of signal peptide cleavage in the Kdap precursor, purified recombinant Kdap-Fc was subjected to N-terminal sequencing. Briefly, 3 d after transfection of pKdap-Fc into COS-1 cells, Fc-fusion proteins in the culture supernatant were allowed to bind to Protein A-agarose (Sigma, St Louis, Missouri), and then eluted sequentially with 150 mM NaCl/50 mM acetate buffer (pH 4.3) and 150 mM NaCl/50 mM glycine buffer (pH 2.3). Fractions with highest protein concentrations were selected and applied to SDS-PAGE, followed by western blotting. A band with reactivity to goat anti-human IgG Ab was purified by gel extraction and subjected to 15 cycles of N-terminal sequencing by automated Edman degradation in the HHMI Protein Chemistry Core Research Facility (UT Southwestern).

Skin samples Biopsies were taken from lesional skin sites of three individuals with psoriasis. Our study was performed after the ethics committee approval and informed consent was obtained under the Declaration of Helsinki Principles. The controls included two normal individuals (one female and one male) without skin disease for fluorescence and for *in situ* hybridization and two different individuals for immunoelectron microscopy (two males).

Indirect immunofluorescence Human skin cryostat sections were fixed in cold acetone (−20°C) for 10 min and incubated with 5% normal goat serum (NGS) in 0.1 M Dulbecco's PBS for 5 min at 37°C. Sections were incubated with anti-Kdap Ab or rabbit control IgG (diluted at 1:50), secondary antibody goat anti-rabbit IgG fluorescein isothiocyanate (FITC, Dako, Kyoto, Japan), diluted in 3% bovine serum albumin (BSA) in 0.1 M PBS for 30 min at 37°C. The sections were then mounted in Permafluor (Thermo Shandon,

Pittsburgh, Pennsylvania) and examined with a Nikon Optiphot 2 microscope equipped for epifluorescence or a confocal laser inverted microscope (Olympus Fluoview FV300 Optical Elements Corporation, Dulles, VA). Images were scanned sequentially using a 40 times objective, and multiple images were Kalman averaged ($n > 5$).

Post-embedding immunogold electron microscopy Skin samples were obtained from the outer aspect of the arm and thigh, and were processed for post-embedding immunoelectron microscopy as previously described (Shimizu *et al*, 1989). Briefly, samples were cryoprotected in 20% glycerol/PBS for 1 h at 4°C, and plunged in liquid propane at −190°C using a KF-80 apparatus (Reichert Jung, Vienna, Austria). After freeze substitution over 3 d at −80°C in methanol and over 2 d at −60°C using the AFS apparatus (Leica, Milton Keynes, UK), the samples were embedded in Lowicryl K11M resin polymerized by UV light. Ultrathin sections were cut and collected on pioloform-coated nickel grids. The sections were pre-incubated in PBS containing 5% NGS, 1% BSA, and 0.1% gelatin and then incubated with anti-Kdap Ab (1:100 dilution) at 37°C for 2 h. After washing with PBS, the sections were incubated with secondary linker Ab for 2 h at 37°C, followed by incubation with a gold-conjugated antibody for 2 h at 37°C. After staining with alcoholic uranyl acetate (15 min) and Reynolds lead citrate (5 s), the sections were observed in a Hitachi H7100-transmission electron microscope (Hitachi, Tokyo, Japan).

***In situ* hybridization of human skin** This assay was performed using manufacturer's recommendations of mRNA *locator* (Ambion, Austin, Texas). Briefly, frozen skin sections were treated with proteinase K at room temperature for 20 min. After fixation, genomic nucleotides were digested with 500 U per mL DNase I at 37°C for 1 h. Control sections were treated with RNase (instead of DNase). For probe preparation, a full-length cDNA of *Kdap* (441 bp) was subcloned into a pGEM-7zf(−) (Promega, Madison, Wisconsin) and used as a template for *in vitro* RNA synthesis using MAXIscript (Ambion). Anti-sense and sense (negative control) RNA probes were synthesized by T7 and SP6, respectively, RNA polymerase in the presence of biotin-labeled UTP (Invitrogen). DNase-treated sections were then hybridized at 42°C for 24 h with 10 ng per mL biotin-labeled RNA probe. After washing, unhybridized Ribo probes were digested with 1 μg per mL RNase A for 30 min at 37°C, and hybridized probes were then visualized by histochemistry using HRP-labeled streptavidin, avidin-peroxidase, and AEC reagent.

We are grateful to Dr Tasuku Honjo for providing pcDL-SRα-Tac(3') expression vector, Irene Dougherty and Hideki Nakamura for technical support, and Susan Milberger for administrative assistance. This research was supported partially by Pilot & Feasible Study Skin Disease Research Core (P30 AR41940-10).

DOI: 10.1111/j.0022-202X.2004.22511.x

Manuscript received August 25, 2003; revised November 18, 2003; accepted for publication December 10, 2003

Address correspondence to: Kiyoshi Ariizumi, Department of Dermatology, UT Southwestern Med. Ctr., 5323 Harry Hines Blvd, Dallas, Texas 75390-9069, USA. Email: kiyoshi.ariizumi@utsouthwestern.edu

References

Ariizumi K, Bergstresser PR, Takashima A: Subtractive cDNA cloning. A new approach to understanding dendritic cell biology In: Dendritic Cells in fundamental and Clinical Immunology, (ed.) Ricciardi-Castagnoli. Plenum Press, New York, 1997; p 449–454

Ariizumi K, Meng Y, Bergstresser PR, Takashima A: IFN-γ-dependent IL-7 gene regulation in keratinocytes. J Immunol 154:6031–6039, 1995

Ariizumi K, Shen G-L, Ritter III R, *et al*: Identification of a novel, dendritic cell-associated molecule, Dectin-1, by subtractive cDNA cloning. J Biol Chem 275:20157–20167, 2000

Bonkobara M, Das A, Takao J, Cruz PDJ, Ariizumi K: Identification of genes for secreted and membrane-anchored proteins in keratinocytes. Br J Dermatol 148:654–664, 2003

Chatterjee S, Mayor S: The GPI-anchor and protein sorting. CMLS Cell Mol Life Sci 58:1969–1987, 2001

Cui CY, Aragane Y, Maeda A, Piao YL, Takahashi M, Kim LH, Tezuka T: Bikunin, a serine protease inhibitor, is present on the cell boundary of epidermis. J Invest Dermatol 113:182–188, 1999

de Viragh PA, Huber M, Hohl D: Involucrin mRNA is more abundant in human hair follicles than normal epidermis. J Invest Dermatol 103:815–819, 1994

Girolomoni G, Stone DK, Bergstresser PR, Crutz PDJ: Increased number and microtubule-associated dispersal of acidic intracellular compartments accompany differentiation of cultured human keratinocytes. J Invest Dermatol 98:911–917, 2000

He TC, Zhou S, Da Costa LT, Yu J, Kinzler KW, Vogelstein B: A simplified system for generating recombinant adenoviruses. Proc Natl Acad Sci USA 95:2509–2514, 1998

Ishida-yamamoto A, Iizuka H: Structural organization of cornified cell envelops and alterations in inherited skin disorders. Exp Dermatol 7:1–10, 1998

Jin F, Nathan C, Radzioch D, Ding A: Secretory leukocyte protease inhibitor: A macrophage product induced by and antagonistic to bacterial lipopolysaccharide. Cell 88:417–426, 1997

Kalinin A, Marekov LN, Steinert PM: Assembly of the epidermal cornified cell envelope. J Cell Sci 114:3069–3070, 2001

Lavker RM, Risse B, Brown H, Ginsburg D, Pearson J, Baker MS, Jensen PJ: Localization of plasminogen activator inhibitor type 2 (PAI-2) in hair and nail: Implications for terminal differentiation. J Invest Dermatol 110: 917–922, 1998

Mägert HJ, Kreutzmann P, Ständker L, Walden M, Drögemüller K, Forssmann WG: LEKTI: A multidomain serine proteinase inhibitor with pathophysiological relevance. Int J Biochem Cell Biol 34:573–576, 2001

Molhuizen HO, Schalkwijk J: Structural, biochemical, and cell biological aspects of the serine proteinase inhibitor SKALP/elafin/ESI. Biol Chem Hoppe Seyler 376:1–7, 1995

Nakane H, Ishida-yamamoto A, Takahashi H, Iizuka H: Elafin, a secretory protein, is cross-linked into the cornified cell envelopes from the inside of psoriatic keratinocytes. J Invest Dermatol 119:50–55, 2002

Oomizu S, Sahuc F, Asahina K, *et al*: Kdap, a novel gene associated with the stratification of the epithelium. Gene 256:19–27, 2000

Pfundt R, van Ruissen F, Vlijmen-Willems IMJJV, *et al*: Constitutive and inducible expression of SKALP/elafin provides anti-elastase defense in human epithelia. J Clin Invest 98:1389–1399, 1996

Schalkwijk J, Chang A, Janssen P, De Jongh GJ, Mier PD: Skin-derived anti-leucoproteases (SKALPs): Characterization of two new elastase inhibitors from psoriatic epidermis. Br J Dermatol 122:631–641, 1990

Schalkwijk J, Wiedow O, Hirose S: The trappin gene family: Proteins defined by an N-terminal transglutaminase substrate domain and a C-terminal four-disulphide core. Biochem J 340:569–577, 1999

Shikano S, Bonkobara M, Zukas PK, Ariizumi K: Molecular cloning of a dendritic cell-associated transmembrane protein, DC-HIL, that promotes RGD-dependent adhesion of endothelial cells through recognition of heparan sulfate proteoglycans. J Biol Chem 276:8125–8134, 2001

Shimizu H, McDonald JN, Kennedy AR, Eady RAJ: Demonstration of intra- and extra-cellular localization of bullous pemphigoid antigen using cryofixation and freeze substitution for postembedding immuno-electron microscopy. Arch Dermatol Res 281:443–448, 1989

Sotiropoulou G, Anisowicz A, Sager R: Identification, cloning, and characterization of cystatin M, a novel cysteine, proteinase inhibitor, down-regulated in breast cancer. J Biol Chem 272:903–910, 1997

Steinert PM, Marekov LN: The proteins elafin, filaggrin, keratin intermediate filaments, loricrin, and small proline-rich proteins 1 and 2 are isodipeptide cross-linked components of the human epidermal cornified cell envelope. J Biol Chem 270:17702–17711, 1995

Takahashi M, Tezuka T, Katunuma N: Phosphorylated cystatin a is a natural substrate of epidermal transglutaminase for formation of skin cornified envelope. FEBS Lett 308:79–82, 1992

Tashiro K, Nakano T, Honjo T: Signal sequence trap, expression cloning method for secreted proteins and type 1 membrane proteins. Methods Mol Biol 69:203–219, 1997

Tashiro K, Tada H, Heilker R, Shirozu M, Nakano T, Honjo T: Signal sequence trap: A cloning strategy for secreted proteins and type I membrane proteins. Science 261:600–602, 1993

Watt FM: Terminal differentiation of epidermal keratinocytes. Curr Opin Cell Biol 1:1107–1115, 2000

Wiedow O, Schroder JM, Gregory H, Young JA, Christophers E: Elafin: An elastase-specific inhibitor of human skin. Purification, characterization, and complete amino acid sequence. J Biol Chem 265:14791–14795, 1990

Wilson IB, Gavel Y, von Heijne G: Amino acid distributions around O-linked glycosylation sites. Biochem J 275:529–534, 1991

Zeeuwen PLJM, Henriks W, de Jong WW, Schalkwijk J: Identification and sequence analysis of two new members of the SKALP/elafin and SPAI-2 gene family. J Biol Chem 272:20471–20478, 1997

Zeeuwen PLJM, Vlijmen-Willems IMJJV, Jansen BJH, *et al*: Cystatin M/E expression is restricted to differentiated epidermal keratinocytes and sweat glands: A new skin-specific proteinase inhibitor that is a target for cross-linking by transglutaminase. J Invest Dermatol 116:693–701, 2001

insight into the role of antimicrobial peptides in relative resistance/susceptibility to bacterial infections associated with inflammatory lesions of the skin.

We are thankful to Drs Eugene M. Farber and Brian J. Nickoloff for their suggestions and intellectual support.

REFERENCES

1. Raychaudhuri SP, Raychaudhuri SK. Relationship between kinetics of lesional cytokines and secondary infection in inflammatory skin disorders: a hypothesis. Int J Dermatol 1993;32:409-12.
2. Ganz T, Selsted ME, Szklarek D, Harwig SS, Daher K, Bainton DF, et al. Defensins: natural peptide antibiotics of human neutrophils. J Clin Invest 1985;76:1427-35.
3. Schroder JM, Harder J. Human beta-defensin-2. Int J Biochem Cell Biol 1999;31:645-51.
4. Krensky AM. Granulysin: a novel antimicrobial peptide of cytolytic T lymphocytes and natural killer cells. Biochem Pharmacol 2000;59:317-20.
5. Stenger S, Hanson DA, Teitelbaum R, Dewan P, Niazi KR, Froelich CJ, et al. An antimicrobial activity of cytolytic T cells mediated by granulysin. Science 1998;282:121-5.
6. Raychaudhuri SP, Jiang WY, Farber EM, Schall TJ, Ruff MR, Pert CB. Upregulation of RANTES in psoriatic keratinocytes: a possible pathogenic mechanism for psoriasis. Acta Derm Venereol 1999;79:9-11.
7. Sing G, Rao DJ. Bacteriology of psoriatic plaques. Dermatologica 1978;157:21-7.
8. Payne RW. Severe outbreak of surgical sepsis due to *Staphylococcus aureus* of uncommon type and origin. Br Med J 1967;4:17-20.
9. Ong PY, Ohtake T, Brandt C, Strickland I, Boguniewicz M, Ganz T, et al. Endogenous antimicrobial peptides and skin infections in atopic dermatitis. N Engl J Med 2002;347:1151-60.
10. Bonish B, Jullien D, Dutronc Y, Huang BB, Modlin R, Spada FM, et al. Overexpression of CD1d by keratinocytes in psoriasis and CD1d-dependent IFN-gamma production by NK-T cells. J Immunol 2000;165:4076-85.
11. Harder J, Bartels J, Christophers E, Schroder JM. A peptide antibiotic from human skin. Nature 1997;387:861.

DNA-based prenatal exclusion of bullous congenital ichthyosiform erythroderma at the early stage, 10 to 11 weeks' of pregnancy, in two consequent siblings

Yukiko Tsuji-Abe, MD,[a] Masashi Akiyama, MD, PhD,[a] Hideki Nakamura,[a] Yasuko Takizawa, DVM, PhD,[b] Daisuke Sawamura, MD, PhD,[a] Kayoko Matsunaga, MD, PhD,[c] Kaoru Suzumori, MD, PhD,[d] and Hiroshi Shimizu, MD, PhD[a]

Sapporo, Tokyo, Toyoake, and Nagoya, Japan

The proband was a Japanese woman with bullous congenital ichthyosiform erythroderma harboring a keratin 10 gene mutation M150T. DNA-based prenatal exclusion of bullous congenital ichthyosiform erythroderma was successfully performed in her two consequent pregnancies using chorionic villus samples at 10 to 11 weeks' gestation, several weeks earlier than the previously reported cases. (J Am Acad Dermatol 2004;51:1008-11.)

From the Departments of Dermatology at Hokkaido University Graduate School of Medicine, Sapporo[a]; Keio University School of Medicine, Tokyo[b]; and Fujita Health University School of Medicine, Toyoake[c]; and Department of Obstetrics and Gynecology, Nagoya City University School of Medicine.[d]

Supported in part by a Grant-in-Aid from the Ministry of Education, Science, Sports, and Culture of Japan (No. 16390312 to M. Akiyama).

Conflicts of interest: None identified.

*Reprint requests: Masashi Akiyama, MD, PhD, Department of Dermatology, Hokkaido University Graduate School of Medicine, North 15, West 7, Kita-ku, Sapporo 060-8638, Japan. E-mail: akiyama@med.hokudai.ac.jp.

0190-9622/$30.00

doi:10.1016/j.jaad.2004.06.020

Bullous congenital ichthyosiform erythroderma (BCIE) (MIM#113800) is a severe autosomal dominant congenital ichthyosis caused by mutations in either the keratin 1 (K1) or the keratin 10 (K10) genes.[1-4] Successful prenatal diagnosis (PNDx) of BCIE by fetal skin biopsy specimen was reported in the 1980s.[5] Because K1 and K10 mutations were identified in patients with BCIE, PNDx by direct gene sequencing is technically possible in BCIE. However, only one report of any DNA-based PNDx and one report of a DNA-based prenatal exclusion of BCIE at 15 weeks' gestation were found in the literature.[6,7] We performed DNA-based prenatal exclusion for the disease BCIE in the

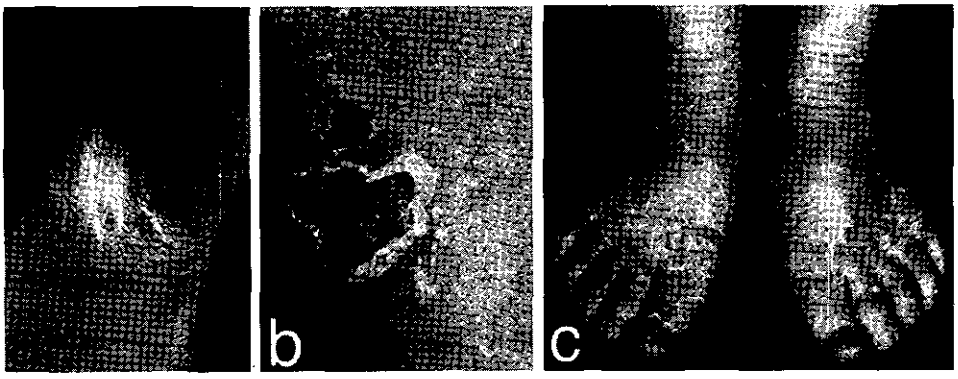

Fig 1. Clinical features of proband. **a**, Hyperkeratosis and scaling of erythematous skin of axilla. **b**, Scales, superficial erosions, and blisters in hyperkeratotic skin were observed on thigh. **c**, Superficial erosions and scales were seen on feet.

two consecutive pregnancies using chorionic villus samples at 10 to 11 weeks' gestation, several weeks earlier than the previously reported cases.

MATERIALS AND METHODS

Case history

A 25-year-old Japanese woman, the proband, showed hyperkeratosis with pigmentation and blisters on her trunk and extremities (Fig 1). She was a sporadic case. Skin biopsy specimen showed the typical granular degeneration and hyperkeratosis. Electron microscopy revealed clumping of keratin filaments in the keratinocytes. From these findings, a diagnosis of BCIE was made and the causative K10 mutation was detected as described below. The details of the proband have been reported previously.[8] One year after the mutation detection, the proband became pregnant for the first time, but the pregnancy resulted in a spontaneous abortion in the early stages of pregnancy. Two years and three years after the first pregnancy, the proband became pregnant two times and the parents requested a PNDx for these pregnancies.

Mutation detection

For mutational analysis of the proband, her husband, and her parents, DNA was isolated from their peripheral blood leukocytes. Domains 1A and 2B of both K1 and K10, and L12 linker domain of K10, were amplified and sequenced. Procedures for mutation detection have been previously described.[8] Specifically, exon 1, which encodes the 1A region of K10, was amplified using the following specific oligonucleotides, 5′-GGAAGCTATGGAAGTAGCAGCT-3′ and antisense, 5′-GCATAGTGAACAGCCACATTGTGC-3′. The mutation was verified by *NIa* III (New England Biolabs Inc, Beverly, Mass) enzyme digestion.

DNA-based prenatal testing

Chorionic villus samples were obtained under ultrasound guidance at 10 to 11 weeks' gestation. Fetal DNA was extracted from the samples, and detection of the *KRT10* mutation was subsequently performed, as described above.

RESULTS

Identification of a missense mutation in the helix initiation motif of K10 in the proband

Direct sequencing of polymerase chain reaction products including exon 1 of *KRT10* revealed a T to C transition at nucleotide position 449 in the proband, compared with the normal sequence. This transition resulted in an amino acid substitution of methionine (ATG) by threonine (ACG) at codon 150 (M150T), which corresponded to the residue 4 of the helix initiation motif of K10. This mutation was reported to be pathogenic[9] and the mutation in the proband had been reported elsewhere.[8] The sequences from the unaffected parents of the proband showed the wild-type sequence at codon 150, thus, M150T was thought to be a sporadic mutation in the proband. The M150T mutation abolished a recognition site of the restriction enzyme *NIa*III. This mutation was not found in 100 alleles from 50 healthy unrelated Japanese individuals using the enzyme digestion method and was not likely to be a polymorphism (data not shown). No pathogenic mutations were detected within the helix initiation and termination motifs of K1 and K10, or the linker domain (L12) of K10, in the proband's DNA.

DNA-based prenatal exclusion in both fetuses

Direct sequencing of polymerase chain reaction products including exon 1 of *KRT10* from the two fetuses of both pregnancies revealed an absence of

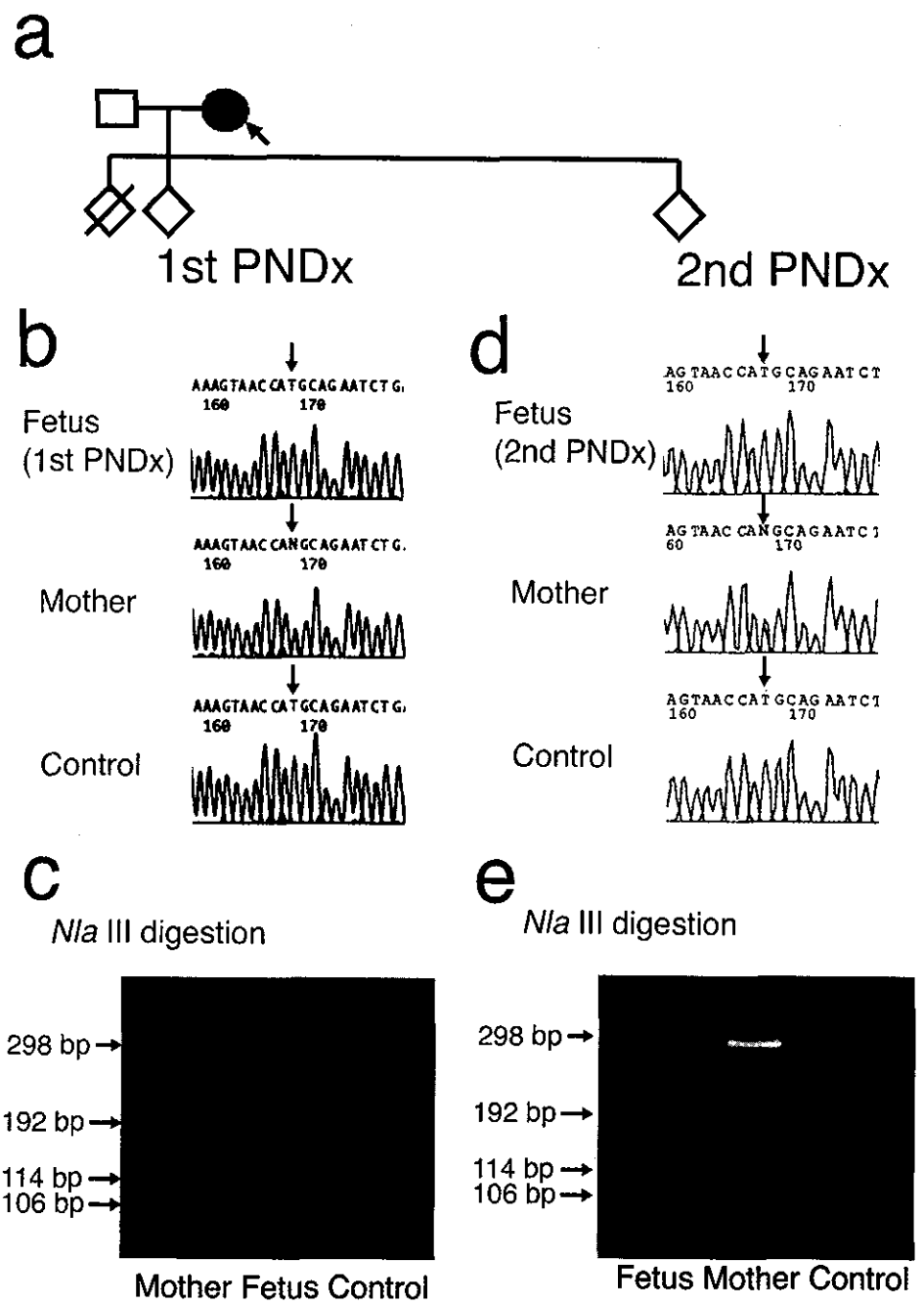

Fig 2. DNA-based prenatal exclusion of fetuses. **a**, Pedigree of fetuses' family. *Arrow*, proband. **b** and **d**, Sequences from genomic DNA of fetuses at risk showed wild-type sequence at codon 150 without pathogenetic missense mutation M150T (first [**a**] and second [**c**] case of prenatal diagnosis [*PNDx*]). Sequences from affected proband showed missense mutation M150T. Sequences from healthy control subject showed wild-type sequence at codon 150. **c** and **e**, Restriction enzyme digestion analysis with *Nla*III revealed that fetuses and healthy control subjects show only 192 bp, 114 bp, 106 bp, and 52 bp bands, although affected proband exhibits an undigested 298 bp band (first [**c**] and second [**e**] case of PNDx).

M150T mutation (Fig 2, *b* and *d*). Digestion by the restriction enzyme NlaIII confirmed the absence of the mutation in the polymerase chain reaction products from the fetuses (Fig 2, *c* and *e*). Thus, both fetuses were judged not to harbor the missense mutation M150T in K10 and were predicted to be healthy. The proband gave birth to healthy girls. The first baby was born weighing in at 3224 g at 40 weeks' and 6 days' gestation and the second baby was 2936 g at 41 weeks' and 5 days' gestation.

DISCUSSION

As the results of current prenatal testing, no mutation was identified in the 1A region of K10 and, in particular, the point mutation found in the affected proband was not present in the two fetuses. It should be noted that the absence of the particular defect does not guarantee the absence of a different spontaneous mutation elsewhere in K1 or K10 genes. However, because of the very low incidence of sporadic cases of BCIE,[10] the probability of BCIE in the fetuses as a result of a different spontaneous mutation was extremely low. In fact, the healthy infants were eventually delivered and had no clinical manifestations of BCIE.

PNDx of BCIE has been successfully performed using ultrastructural observations of fetal skin biopsy samples and amniotic fluid cells,[5,11] and by direct gene sequencing of chorionic villus samples.[6] The major advantage of DNA-based PNDx is that it can be performed at a much earlier stage of pregnancy than PNDx by fetal skin biopsy specimen. Especially in keratinization disorders, the disease phenotype becomes apparent usually at a later stage of pregnancy after the morphologic changes of keratinization have started, and PNDx by fetal skin biopsy specimen is available only at that late stage. Keratinization of the interfollicular epidermis does not begin until later, and the earliest reported age for PNDx of BCIE by fetal skin biopsy specimen is 19 weeks' gestation.[12] On the contrary, direct gene sequencing from chorionic villus samples can be done as early as 8 weeks' gestation. The earliest previously reported age for the PNDx of BCIE was 15 weeks. In the reported fetuses at risk, prenatal exclusion was performed successfully using chorionic villus samples at 10 to 11 weeks' gestation, the earliest gestational age reported in the prenatal testing for BCIE. The early exclusion of BCIE might be beneficial in reducing the burden of the ongoing physical and mental stress on the mother.

We thank Ms Kaori Sakai for her excellent technical assistance and Dr James R. McMillan for the proofreading of this manuscript.

REFERENCES

1. Cheng J, Syder AJ, Yu Q-Y, Letai A, Paller AS, Fuchs E. The genetic basis of epidermolytic hyperkeratosis: a disorder of differentiation-specific epidermal keratin genes. Cell 1992;70:811-9.
2. Chipev CC, Korge BP, Markova N, Bale SJ, DiGiovanna JJ, Compton JC, et al. A leucine-proline mutation in the H1 subdomain of keratin 1 causes epidermolytic hyperkeratosis. Cell 1992;70:621-8.
3. Rothnagel JA, Dominey AM, Dempsey LD, Longley MA, Greenhalg DA, Gagne TA, et al. Mutations in the rod domains of keratins 1 and 10 in epidermolytic hyperkeratosis. Science 1992;257:1128-30.
4. Leigh IM, Lane EB. Mutations in the genes for epidermal keratins in epidermolysis bullosa and epidermolytic hyperkeratosis. Arch Dermatol 1993;129:1571-7.
5. Golbus MS, Sagebiel RW, Filly RA, Gindhart TD, Hall YG. Prenatal diagnosis of congenital bullous ichthyosiform erythroderma (epidermolytic hyperkeratosis) by fetal skin biopsy. N Engl J Med 1980;302:93-5.
6. Rothnagel JA, Longley MA, Holder RA, Küster W, Roop DR. Prenatal diagnosis of epidermolytic hyperkeratosis by direct gene sequencing. J Invest Dermatol 1994;102:13-6.
7. Rothnagel JA, Lin MT, Longley MA, Holder RA, Hazen PG, Levy ML, et al. Prenatal diagnosis for keratin mutations to exclude transmission of epidermolytic hyperkeratosis. Prenat Diagn 1998;18:826-30.
8. Akiyama M, Takizawa Y, Sawamura D, Matsuo I, Shimizu H. Disruption of the suprabasal keratin network by mutation M150T in the helix initiation motif of keratin 10 does not affect cornified cell envelope formation in human epidermis. Exp Dermatol 2003;12:638-45.
9. Paller AS, Syder AJ, Chan YM, Yu QC, Hutton E, Tadini G, et al. Genetic and clinical mosaicism in a type of epidermal nevus. N Engl J Med 1994;331:1408-15.
10. Griffiths WAD, Judge MR, Leigh IM. Bullous ichthyosiform erythroderma. In: Champion RH, Burton JL, Burns DA, Breathnach SM, editors. Textbook of dermatology. 6th ed. Oxford: Blackwell Science; 1998. p. 1504-8.
11. Eady RA, Gunner DB, Carbone LD, Bricarelli FD, Gosden CM, Rodeck CH. Prenatal diagnosis of bullous ichthyosiform erythroderma: detection of tonofilament clumps in fetal epidermal and amniotic fluid cells. J Med Genet 1986;23:46-51.
12. Sybert VP, Holbrook KA, Levy M. Prenatal diagnosis of severe dermatologic diseases. Adv Dermatol 1992;7:179-209.

American Journal of Pathology, Vol. 165, No. 6, December 2004

Tumorigenesis and Neoplastic Progression

Minodronate, a Newly Developed Nitrogen-Containing Bisphosphonate, Suppresses Melanoma Growth and Improves Survival in Nude Mice by Blocking Vascular Endothelial Growth Factor Signaling

Sho-ichi Yamagishi,* Riichiro Abe,† Yosuke Inagaki,* Kazuo Nakamura,* Hiroshi Sugawara,† Daisuke Inokuma,† Hideki Nakamura,† Tadamichi Shimizu,† Masayoshi Takeuchi,‡ Akihiko Yoshimura,§ Richard Bucala,¶ Hiroshi Shimizu,† and Tsutomu Imaizumi*

From the Department of Internal Medicine III, Kurume University School of Medicine, Kurume, Japan; the Department of Dermatology,† Hokkaido University School of Medicine, Sapporo, Japan; the Department of Biochemistry,‡ Hokuriku University, Kanazawa, Japan; the Division of Molecular and Cellular Immunology,§ Medical Institute of Bioregulation, Kyushu University, Fukuoka, Japan; and the Departments of Medicine and Pathology,¶ Yale University School of Medicine, New Haven, Connecticut*

Angiogenesis, a process by which new vascular networks are formed from pre-existing capillaries, is required for tumors to grow, invade, and metastasize. Vascular endothelial growth factor (VEGF), a specific mitogen to endothelial cells, is a crucial factor for tumor angiogenesis. In this study, we investigated whether minodronate, a newly developed nitrogen-containing bisphosphonate, could inhibit melanoma growth and improve survival in nude mice by suppressing the VEGF signaling. We found here that minodronate inhibited melanoma growth and improved survival in nude mice by suppressing the tumor-associated angiogenesis and macrophage infiltration. Minodronate completely inhibited the VEGF-induced increase in DNA synthesis and tube formation in endothelial cells by suppressing NADPH oxidase-mediated reactive oxygen species generation and Ras activation. Furthermore, minodronate inhibited the VEGF-induced expression of intercellular adhesion molecule-1 and monocyte chemoattractant protein-1 in endothelial cells. Minodronate decreased DNA synthesis and increased apoptotic cell death of cultured melanoma cells as well. Our present study suggests that minodronate might suppress melanoma growth and improve survival in nude mice by two independent mechanisms; one is by blocking the VEGF signaling in endothelial cells, and the other is by inducing apoptotic cell death of melanoma. The present study provides a novel potential therapeutic strategy for the treatment of melanoma. *(Am J Pathol 2004, 165:1865–1874)*

Tumors cannot grow beyond a volume of 1 to 2 mm^3 without establishing a vascular supply because cells must be within 100 to 200 μm of a blood vessel to survive.[1,2] A major event in tumor growth and expansion is the angiogenic switch, an alteration in the balance of proangiogenic and anti-angiogenic molecules that leads to tumor neovascularization.[3] Several lines of evidence implicate vascular endothelial growth factor (VEGF) as the key factor involved in angiogenic switch in human tumors.[4] VEGF and its receptors are expressed at high levels in almost all tumors,[4] and administration of antibodies (Abs) directed against VEGF or dominant-negative forms of the VEGF receptor *flk-1* inhibited tumor growth in nude mice.[5,6] Tumor vessels are genetically stable and less likely to accumulate mutations that allow them to develop drug resistance in a rapid manner.[7] Therefore, targeting the VEGF signaling in neovascula-

Supported in part by grants from Venture Research and Development Centers from the Ministry of Education, Culture, Sports, Science, and Technology, Japan (to S.Y.); and by grants-in-aid for scientific research from the Japan Society for the Promotion of Science (to R.A.).

Accepted for publication August 12, 2004.

Address reprint requests to Dr. Sho-ichi Yamagishi, Department of Internal Medicine III, Kurume University School of Medicine, 67 Asahi-machi, Kurume 830-0011, Japan. E-mail: shoichi@med.kurume-u.ac.jp.

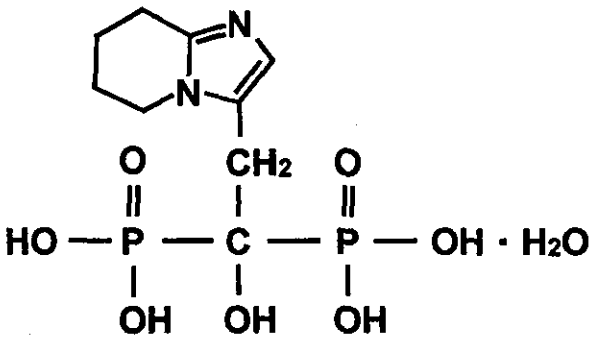

Figure 1. Chemical structure of minodronate. Molecular weight is 340.16.

tures that support tumor growth is considered to be a promising approach to anti-tumor therapy.

Bisphosphonates are potent inhibitors of bone resorption and are widely used drugs for treatment of osteoporosis and osteolytic bone metastasis.[8] *In vitro* anti-tumor properties of bisphosphonates include inhibition of tumor proliferation and invasion and induction of apoptosis of various cancer cell lines.[9,10] Recently, farnesyl pyrophosphate (FPP) synthase has been shown as a molecular target of nitrogen-containing bisphosphonates, and inhibition of posttranslational prenylation of small molecular weight G proteins is likely involved in their anti-resorptive activity on osteoclasts.[11] Bisphosphonates have been reported to accumulate in human vessels.[12] Furthermore, nitrogen-containing bisphosphonates such as ibandronate and zoledronic acid have been shown to inhibit angiogenesis *in vitro*.[13] These observations suggest that nitrogen-containing bisphosphonates might have pleiotropic properties on endothelial cells (ECs) by blocking isoprenoid intermediates, which serve as lipid attachments for a variety of intracellular signaling molecules.[14]

NADPH oxidase activity is required for the angiogenic signaling of VEGF,[15] and small G protein Rac is a critical component of the endothelial NADPH oxidase complex.[16] Further, VEGF is a key factor for melanoma angiogenesis and macrophage infiltration, the extent of which being correlated with tumor prognosis.[17,18] These observations led us to examine whether minodronate, a newly developed nitrogen-containing bisphosphonate, could inhibit melanoma growth and improve survival in nude mice by suppressing the tumor-associated angiogenesis and macrophage infiltration *in vivo*. We also investigated in the present study whether and how minodronate could block the VEGF signaling in ECs.

Materials and Methods

Growth of G361 Xenografts in Nude Mice

One million G361 cells were injected intradermally into the upper flank of 6-week-old female athymic nude mice (n = 5 in each group). Mice received intraperitoneal injections of 5 μg of minodronate (Yamanouchi Pharmaceutical Co., Tokyo, Japan) or physiological saline solution daily. The chemical structure of minodronate is shown in Figure 1. Its molecular weight is 340.16. The smallest and largest diameters of tumors were measured at 5-day intervals with a digital caliper, and tumor volumes were calculated using the following formula: volume (mm^3) = [(smallest diameter)^2 × (largest diameter)]/2. All animal procedures were conducted according to the guidelines provided by the Hokkaido University Institutional Animal Care and Use Committee under an approved protocol.

Immunofluorescence Staining of Tumor Vessels and Macrophages

Five cryostat sections of tumor xenograft were stained with fluorescein isothiocyanate-conjugated rat anti-mouse CD31 or Mac-3 Abs (Becton Dickinson, Franklin Lakes, NJ) as described previously.[19] Nuclei were stained with propidium iodide. Three different fields at ×60 magnification were examined on each section with confocal laser-scanning fluorescence microscopy. Green fluorescence-positive area in three different fields of each section was measured.

Assay for in Situ Apoptosis

Sections of tumor xenograft were stained with hematoxylin and eosin for morphological analysis. Terminal dUTP nick-end labeling assay was performed using an *in situ* apoptosis detection kit according to the manufacturer's instructions (Roche Diagnostics GmbH, Mannheim, Germany). The number of apoptotic cells was counted in 10 randomly selected fields at ×200 magnification using confocal laser-scanning fluorescence microscopy.

Cell Culture Conditions

The human adult skin microvascular ECs were incubated in endothelial cell basal medium (EBM) medium (Clonetics Corp., San Diego, CA) supplemented with 5% fetal bovine serum and 0.4% bovine brain extracts in the presence or absence of 10 ng/ml VEGF (PeproTech, London, UK), 10 μmol/L (3.4 μg/ml) minodronate, 100 nmol/L diphenylene iodonium (DPI) (Sigma, St. Louis, MO), 1 μg/ml geranylgeranyl pyrophosphate (GGPP) (Sigma), 10 μmol/L FTI-276 (Calbiochem, San Diego, CA), 1 μmol/L GGTI-286 (Calbiochem), 1 mmol/L *N*-acetylcysteine (Sigma), 1 μg/ml monoclonal Abs (mAbs) against human intercellular adhesion molecule-1 (ICAM-1) (R&D Systems, Minneapolis, MN), dominant-negative human Rac-1 mutant (DN-RacT17N), or dominant-negative human Ras mutant (DN-RasS17N). G361 melanoma cells (American Type Culture Collection, Manassas, VA) were incubated in Dulbecco's modified Eagle's medium supplemented with 10% fetal bovine serum and 100 U/ml penicillin/streptomycin in the presence or absence of various concentrations of minodronate or 0.5 μg/ml FPP (Sigma).

Intracellular Reactive Oxygen Species (ROS) Generation

Intracellular ROS generation was detected by using the fluorescent probe CM-H_2DCFDA (Molecular Probes Inc., Eugene, OR) as described previously.[20] Briefly, cells (2×10^4/96-well-plate) were loaded with 10 μmol/L CM-H_2DCFDA, incubated for 45 minutes at 37°C, and analyzed in a Fluoroskan Ascent FL (Thermo Labsystems, Helsinki, Finland) using the Ascent Software for Windows program.

In Situ *ROS Generation in Tumor ECs*

The oxidative fluorescent probe dihydroethidium (Molecular Probes Inc.) was used to detect *in situ* levels of ROS in tumor ECs according to the method of Miller and colleagues.[21] Briefly, the unfixed frozen tissues were cut into 10-μm-thick sections. The sections were stained with fluorescein isothiocyanate-conjugated rat anti-mouse CD31 Abs (Beckton Dickinson) and then with 2 μmol/L dihydroethidium. Three different fields at ×60 magnification were examined on each section with confocal laser-scanning fluorescence microscopy. Red fluorescence-positive area in three different fields of each section was measured.

Transfection of DN-RacT17N and DN-RasS17N

The DN-RacT17N expression vector was kindly provided by Dr. Y. Horiguchi, Department of Bacterial Toxicology, Research Institute for Microbial Diseases, Osaka University, Osaka, Japan. The DN-RasS17N expression vector was kindly provided by Dr. T. Sato, Faculty of Bioscience and Biotechnology, Tokyo Institute of Technology, Tokyo, Japan. ECs were transiently transfected with either DN-RacT17N, DN-RasS17N or an empty vector using Tfx-50 reagent according to the manufacture's instructions (Promega, Madison, WI).

Measurement of [^{3}H]Thymidine Incorporation in ECs

[^{3}H]Thymidine incorporation in cells was determined as described previously.[22]

Assay for Ras Activation

ECs were incubated with or without 10 ng/ml VEGF for 24 hours in the presence or absence of 10 μmol/L minodronate or 100 nmol/L DPI. Ras activity then was measured using a Ras Activation Assay kit (Upstate Biotechnology Inc., Charlottesville, VA) following the manufacturer's instructions.

Assay for in Vitro *Tube Formation*

In vitro tube formation was assayed as described previously.[23] Briefly, wells of 24-well culture cluster dishes (Costar 3524; Costar, Cambridge, MA) were coated with Matrigel solution (250 μl/well; Beckton Dickinson, Bedford, MA), then allowed to solidify for at least 1 hour at 37°C. ECs (4×10^4 cells/well) were then seeded on Matrigel with 10 ng/ml of VEGF in the presence or absence of 10 μmol/L minodronate. After 6 hours, four microscopic fields selected at random were photographed, and the lengths of capillary-like structures were measured. The vessel structures were confirmed by electron microscopic analysis.

Primers and Probes

Primer sequences used in semiquantitative reverse transcriptase-polymerase chain reactions (RT-PCRs) were 5′-AATGGGGCTGGGACTTCTCATTGG-3′ and 5′-GCCTGGGTGACAGAGCGAGAGCTT-3′ for human ICAM-1 mRNA, and 5′-AACTGAAGCTCGCACTCTCG-3′ and 5′-TCAGCACAGATCTCCTTGGC-3′ for human monocyte chemoattractant protein-1 (MCP-1) mRNAs. Sequences of the upstream and downstream primers used in RT-PCR for detecting β-actin mRNAs were the same as described previously.[24]

Semiquantitative RT-PCR

Poly(A)$^+$ RNAs were isolated from cells, and analyzed by RT-PCR as described previously.[25] The amounts of poly(A)$^+$ RNA templates (30 ng) and cycle numbers (33 cycles for ICAM-1 gene; 30 cycle for MCP-1 gene; 22 cycles for β-actin gene) for amplification were chosen in quantitative ranges, in which reactions proceeded linearly, that had been determined by plotting signal intensities as functions of the template amounts and cycle numbers.[25]

Assay of MOLT-3 Cell Adhesion to ECs

Molt-3 cell adhesion to ECs was assayed according to the method of de Clerck and colleagues.[26] Briefly, ECs were treated with 10 ng/ml of VEGF in the presence or absence of 10 μmol/L minodronate or 1 μg/ml ICAM-1 mAbs for 24 hours, and then incubated with BCECF-AM-labeled Molt-3 cells for 30 minutes. After incubation, the cells were solubilized by 1% Triton X-100 and the fluorescent intensities of the cells were measured.

Measurement of MCP-1

MCP-1 proteins released into media were measured with an enzyme-linked immunosorbent assay (ELISA) system according to the manufacturer's instructions (R&D Systems).

Assay for in Vitro *Apoptosis*

G361 cells were incubated with the indicated concentrations of minodronate in the presence or absence of 0.5 μg/ml of FPP for 24 hours. Then the cells were lysed and

the supernatant was analyzed in an ELISA for DNA fragments (Cell Death Detection ELISA; Roche Molecular Biochemicals, Mannheim, Germany) according to the manufacturer's instructions.

Statistical Analysis

All values were presented as means ± SE. Unless otherwise indicated, one-way analysis of variance followed by the Scheffé *F*-test, was performed for statistical comparisons. In Figure 2, A, C, D, and E, and Figure 3C, unpaired *t*-test was performed for comparison between control and minodronate-treated groups; $P < 0.05$ was considered significant.

Results

Minodronate Inhibits Melanoma Growth and Improves Survival in Nude Mice

Because minodronate has been reported to dose dependently reduce osteolytic bone metastases in nude mice at the range of 0.2 to 20 μg/mouse/day,[27] we chose the dose of 5-μg daily injection of minodronate in our animal experiments. We first investigated whether minodronate could inhibit melanoma growth in nude mice. G361 xenograft melanoma cells formed rapidly growing tumors in nude mice, reaching 500 to 600 mm^3 after 40 days. In contrast, intraperitoneal daily injection of 5 μg of minodronate almost completely inhibited the *in vivo* tumor growth of G361 cells throughout an observation period of up to 40 days (Figure 2, A and B).

Tumor-associated angiogenesis and macrophage infiltration have been known to play an important role in tumor growth and expansion *in vivo*.[28,29] So, we next studied the effects of minodronate on angiogenesis and macrophage infiltration in G361 melanoma xenografts. Minodronate treatment was found to significantly inhibit tumor-associated angiogenesis and macrophage infiltration in nude mice (Figure 2, C and D, respectively). These observations suggest that minodronate might inhibit melanoma growth in nude mice by blocking the tumor-associated angiogenesis and macrophage infiltration *in vivo*.

Tumors cannot survive without establishing a vascular supply.[1,2] Histological examinations revealed extensive areas of tumor necrosis in minodronate-treated G361 xenograft (Figure 2E). Furthermore, apoptotic cell death of melanoma xenografts was significantly increased by the treatment of minodronate. The Kaplan-Meier analysis showed that the rate of host mouse survival was significantly higher in minodronate-treated group than that in the control group (Figure 2F). None of the minodronate-treated mice died throughout an observation period of up to 100 days.

Minodronate Inhibits VEGF-Induced ROS Generation in ECs

VEGF is a key factor for tumor angiogenesis and macrophage infiltration, thus being involved in melanoma growth and progression.[17,18,30] Because ROS generation is reported to be required for the VEGF signaling in ECs,[31] we first studied whether minodronate could inhibit the ROS generation elicited by VEGF. After the intraperitoneal administration of 5 μg of minodronate, its peak plasma concentration reaches ~10 μmol/L (unpublished data). Therefore, we did the following *in vitro* experiments with minodronate at the concentration of 10 μmol/L. Minodronate or DPI, an inhibitor of NADPH oxidase, completely inhibited the VEGF-induced ROS production in ECs (Figure 3A). Further, the inhibitory effect of minodronate on ROS generation was completely reversed by GGPP. These results suggest that VEGF induces ROS generation through NADPH oxidase and that minodronate inhibits the ROS generation by suppressing geranylgeranylation of Rac, one of the important components of NADPH oxidase complex.[16] Pharmacological inhibitors are not absolutely specific to one cellular target. Because DPI can inhibit other superoxide generating enzymes, we performed experiments using molecular techniques. Overexpression of DN-RacT17N also prevented the increase of ROS generation in VEGF-exposed ECs (Figure 3B). These observations also indicate that Rac is directly involved in the VEGF-induced ROS production in microvascular ECs. Minodronate treatment was also found to decrease *in situ* ROS generation in tumor ECs (Figure 3C). Thus, minodronate exerts antioxidative effects on ECs of tumor-associated blood vessels probably by blocking the VEGF signaling *in vivo*.

Minodronate Inhibits VEGF-Induced DNA Synthesis and Tube Formation in ECs

We next investigated a functional role of NADPH oxidase-mediated ROS generation in VEGF-induced angiogenesis. DPI or an anti-oxidant, *N*-acetylcysteine, completely inhibited the VEGF-induced increase in DNA synthesis, suggesting that NADPH oxidase-derived ROS is involved in the VEGF signaling to angiogenesis (Figure 4A). Inactivation of Rac by 10 μmol/L minodronate or a geranylgeranyltransferase inhibitor, GGTI-286, or overexpression of DN-RacT17N also prevented the VEGF effect, thus demonstrating that geranylgeranylation of Rac is necessary for the angiogenic signals of VEGF (Figure 4, B and C). However, in contrast to the case with ROS production, the effect of minodronate on DNA synthesis was not reversed by GGPP. These results suggest that inactivation of other G proteins might also be involved in the anti-angiogenic effects of minodronate. Minodronate at lower concentrations (0.1 and 1 μmol/L) did not affect DNA synthesis in ECs, irrespective of the presence or absence of VEGF (data not shown). These findings suggest that, unlike the effects of statins, minodronate does not have biphasic actions on DNA synthesis in ECs at the concentrations of 0.1 to 10 μmol/L.[32] Furthermore, minodronate did not induce apoptotic cell death in ECs exposed to VEGF (data not shown).

We next examined the involvement of Ras in the VEGF signaling to angiogenesis. VEGF was found to activate Ras in microvascular ECs, which was completely pre-

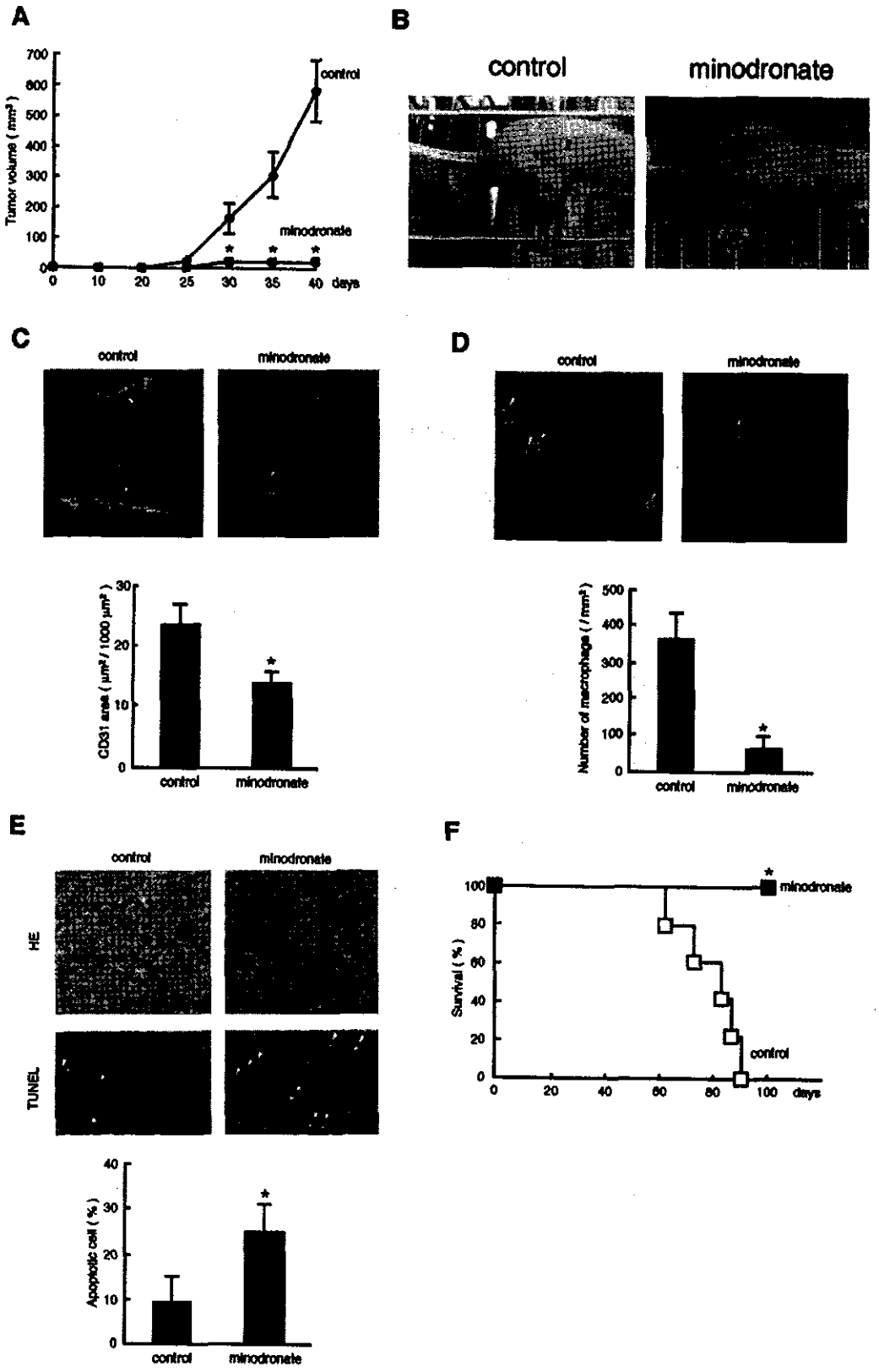

Figure 2. Effects of minodronate on tumor growth (**A** and **B**), angiogenesis (**C**), macrophage infiltration (**D**), apoptosis (**E**), and survival rate (**F**) in nude mice. **A:** Each group (minodronate-treated or nontreated control group) was composed of five athymic nude mice. **B:** Typical photographs were taken after 40 days of injection. **Arrowheads** indicate tumors. **C:** Five cryostat sections of tumor xenograft were stained. Green fluorescence-positive areas in three different fields of each section were measured. **Arrowheads** indicate CD31-positive ECs (green). **D: Arrowheads** indicate Mac-3-positive macrophages (green). **E:** The number of apoptotic cells was counted in 10 randomly selected fields. **Arrowheads** indicate apoptotic cells (green). Tumor nuclei were stained in red. *, $P < 0.01$ compared to control mice. **F:** Kaplan-Meier analysis.

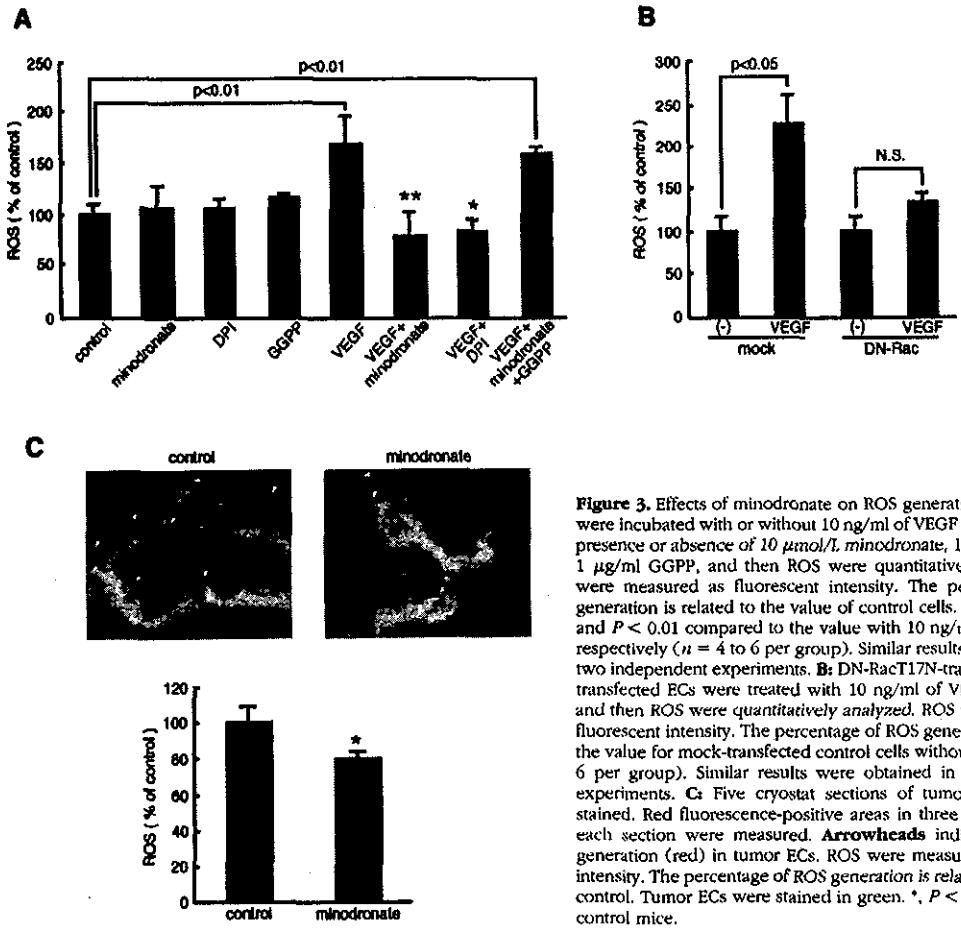

Figure 3. Effects of minodronate on ROS generation in ECs. **A:** ECs were incubated with or without 10 ng/ml of VEGF for 24 hours in the presence or absence of 10 μmol/L minodronate, 100 nmol/L DPI, or 1 μg/ml GGPP, and then ROS were quantitatively analyzed. ROS were measured as fluorescent intensity. The percentage of ROS generation is related to the value of control cells. * and **, $P < 0.05$ and $P < 0.01$ compared to the value with 10 ng/ml of VEGF alone, respectively ($n = 4$ to 6 per group). Similar results were obtained in two independent experiments. **B:** DN-RacT17N-transfected or mock-transfected ECs were treated with 10 ng/ml of VEGF for 24 hours, and then ROS were quantitatively analyzed. ROS were measured as fluorescent intensity. The percentage of ROS generation is related to the value for mock-transfected control cells without VEGF ($n = 4$ to 6 per group). Similar results were obtained in two independent experiments. **C:** Five cryostat sections of tumor xenograft were stained. Red fluorescence-positive areas in three different fields of each section were measured. **Arrowheads** indicate *in situ* ROS generation (red) in tumor ECs. ROS were measured as fluorescent intensity. The percentage of ROS generation is related to the value of control. Tumor ECs were stained in green. *, $P < 0.05$ compared to control mice.

vented by minodronate or DPI (Figure 4D). Further, inactivation of Ras by a farnesyltransferase inhibitor, FTI-276, or overexpression of DN-RasS17N also inhibited the increase in DNA synthesis in VEGF-exposed ECs (Figure 4, E and F). These observations suggest that Ras is a downstream effector of ROS derived form NADPH oxidase and that the anti-angiogenic effects of minodronate can be attributed to inhibition of both Rac and Ras prenylation.

The process of angiogeneis is completed by the formation of microvascular tubes.[23] *In vitro* assays for tube formation of ECs have been developed and used to study this critical step of angiogenesis. Therefore, we further studied the effect of minodronate on tube formation on Matrigel, where ECs take only several hours to associate with each other and to form microtubes.[23] Minodronate completely prevented the VEGF-induced tube formation on Matrigel (Figure 4G). These observations suggest that minodronate could inhibit tube formation of microvascular ECs, the key steps of angiogenesis by blocking the VEGF signaling as well.

Minodronate Inhibits VEGF-Induced ICAM-1 and MCP-1 Overexpression in ECs

VEGF also acts as a proinflammatory cytokine.[33,34] To determine whether minodronate could block the proinflammatory signals of VEGF, we investigated the effects of minodronate on ICAM-1 and MCP-1 expression in VEGF-exposed ECs. Minodronate completely inhibited the VEGF-induced up-regulation of ICAM-1 and MCP-1 mRNA levels in microvascular ECs (Figure 5A). Because our RT-PCR analyses are semiquantitative, to confirm the mRNA findings, we did leukocyte adhesion assay and MCP-1 ELISA. Minodronate inhibited ICAM-1-mediated Molt-3 cell adhesion to, and MCP-1 overproduction in, microvascular ECs (Figure 5, B and C). Cell-based ELISA confirmed that VEGF actually induced ICAM-1 protein expression, which was completely blocked by minodronate (data not shown). GGTI-286 or FTI-276, a geranylgeranyltransferase or farnesyltransferase inhibitor, respectively, also inhibited the VEGF-induced up-regulation of ICAM-1 and MCP-1 (data not shown), suggesting the involvement of both Rac and Ras in the VEGF signaling to inflammation as well.

Minodronate Inhibits DNA Synthesis and Induces Apoptosis in Cultured G361 Melanoma Cells

We next investigated the direct effects of minodronate on DNA synthesis and apoptotic cell death of cultured G361 cells *in vitro*. Minodronate was found to decrease DNA

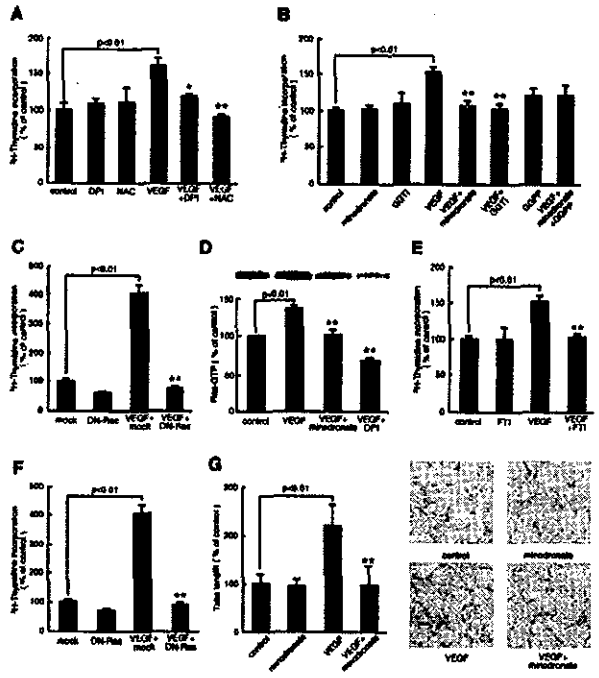

Figure 4. Effects of minodronate on growth and tube formation of microvascular EC. **A**, **B**, and **E**: ECs were incubated with or without 10 ng/ml of VEGF for 24 hours in the presence or absence of 100 nmol/L DPI, 1 mmol/L *N*-acetylcysteine, 10 μmol/L minodronate, 1 μmol/L GGTI-286, 1 μg/ml GGPP, or 10 μmol/L FTI-276, and then [^{3}H]thymidine incorporation was measured. The percentage of [^{3}H]thymidine incorporation is related to the value of the control. One hundred percent indicates 25,743 cpm. **C** and **F**: DN-RacT17N-, DN-RasS17N-, or mock-transfected ECs were treated with 10 ng/ml of VEGF for 24 hours, and then [^{3}H]thymidine incorporation was measured. The percentage of [^{3}H]thymidine incorporation is related to the value of mock-transfected cells without VEGF. One hundred percent indicates 5623 cpm. **D**: Ras activity. ECs were incubated with or without 10 ng/ml of VEGF for 24 hours in the presence or absence of 10 μmol/L minodronate or 100 nmol/L DPI. The percentage of band density is related to the value of the control. **G**: ECs were seeded on Matrigel and incubated with or without 10 ng/ml of VEGF for 6 hours in the presence or absence of 10 μmol/L minodronate. The percentage of length is related to the value of the control. One hundred percent indicates 4.65 mm/mm^2. * and **, $P < 0.05$ and $P < 0.01$ compared to the value with 10 ng/ml of VEGF alone, respectively (n = 4 to 6 per group). Similar results were obtained in two independent experiments.

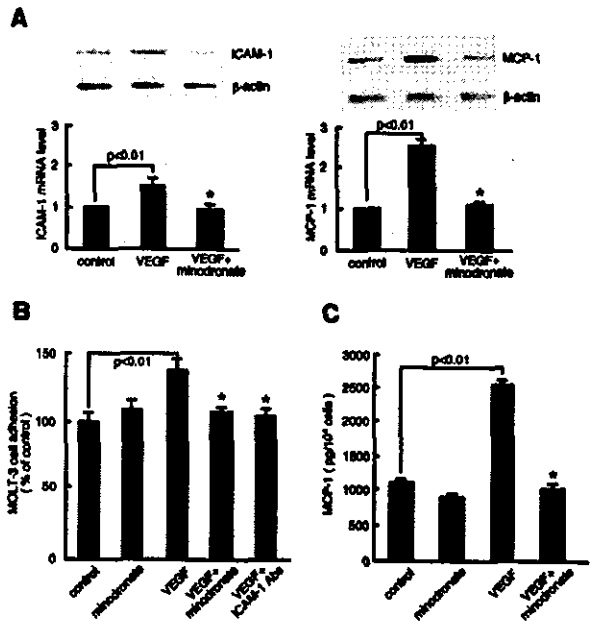

Figure 5. Effects of minodronate on ICAM-1 and MCP-1 expression in VEGF-exposed ECs. **A**: ECs were incubated with or without 10 ng/ml of VEGF for 4 hours in the presence or absence of 10 μmol/L minodronate. Thirty ng of poly(A)$^+$ RNAs were transcribed and amplified by PCR. Each **bottom** panel shows quantitative representation of ICAM-1 and MCP-1 gene induction. Data are normalized by the intensity of β-actin mRNA-derived signals and then related to the value of the control. **B**: ECs were incubated with or without 10 ng/ml of VEGF for 24 hours in the presence or absence of 10 μmol/L minodronate or 1 μg/ml of mAbs against human ICAM-1. Molt-3 cell adhesion was measured as fluorescent intensity. The percentage of Molt-3 cell adhesion is related to the value of control cells. **C**: MCP-1 content in the medium was measured. *, $P < 0.01$ compared to the value with VEGF alone (n = 4 to 6 per group). Similar results were obtained in two independent experiments.

synthesis and increase apoptotic cell death of melanoma cells in a dose-dependent manner (Figure 6, A and B). Minodronate at 10 μmol/L, which effectively blocked the VEGF signaling in cultured ECs, significantly induced apoptotic cell death of melanoma cells, whose effects were completely reversed by the addition of 0.5 μg/ml of FPP (Figure 6C). GGPP at 1 μg/ml did not affect the proapoptotic effects of minodronate *in vitro* (data not shown). These results suggest that minodronate could act on melanoma cells directly to induce apoptosis via suppression of Ras farnesylation.

Discussion

We demonstrated in the present study for the first time that minodronate, a nitrogen-containing bisphosphonate, suppressed melanoma growth and improved survival in nude mice by blocking the tumor-associated angiogenesis and macrophage infiltration. We also found here that minodronate blocked the VEGF signaling to angiogenesis and inflammation in microvascular ECs by suppressing NADPH oxidase-mediated ROS generation and Ras activation. Minodronate has previously been shown to inhibit osteolytic bone metastases of human small-cell lung cancer in natural killer cell-depleted severe combined immunodeficient mice.[35,36] The present study has extended these previous works, thus suggesting that minodronate could be a promising anti-melanoma drug as well.

Several lines of evidence implicate VEGF as the key factor involved in melanoma growth and metastasis.[4] VEGF expression levels are associated with angiogenesis and macrophage infiltration, the extent of which being correlated with melanoma prognosis.[17,18,30] Our present study suggests that minodronate might inhibit melanoma growth and expansion by blocking the VEGF signaling *in vivo*. Figure 7 illustrates a proposed scheme, by which VEGF promotes growth and expansion in melanoma xenografts; VEGF might induce the tumor-associated angiogenesis and macrophage infiltration through NADPH oxidase-mediated ROS generation and Ras activation in ECs. Minodronate could block the VEGF signaling via inhibition of protein prenylation of both Rac and Ras, thus suppressing melanoma growth and subsequently improving survival in nude mice. In our present study, the effects of minodronate on VEGF-induced ROS genera-